© 2017. Published by The Company of Biologists Ltd | Development (2017) 144, 2392-2401 doi:10.1242/dev.149757

RESEARCH ARTICLE

Placental labyrinth formation in mice requires endothelial FLRT2/UNC5B signaling

Ikue Tai-Nagara[1,*], Yusuke Yoshikawa[1,2,*], Naoko Numata[1], Tomofumi Ando[1,2], Keisuke Okabe[1,3], Yuki Sugiura[4], Masaki Ieda[5], Nobuyuki Takakura[6], Osamu Nakagawa[7], Bin Zhou[8], Koji Okabayashi[2], Makoto Suematsu[4], Yuko Kitagawa[2], Martin Bastmeyer[9], Kohji Sato[10], Rüdiger Klein[11,12], Sutip Navankasattusas[13], Dean Y. Li[13,14,15,16,17,18,19], Satoru Yamagishi[10,*,‡] and Yoshiaki Kubota[1,*,‡]

ABSTRACT

The placental labyrinth is the interface for gas and nutrient exchange between the embryo and the mother; hence its proper development is essential for embryogenesis. However, the molecular mechanism underlying development of the placental labyrinth, particularly in terms of its endothelial organization, is not well understood. Here, we determined that fibronectin leucine-rich transmembrane protein 2 (FLRT2), a repulsive ligand of the UNC5 receptor family for neurons, is unexpectedly expressed in endothelial cells specifically in the placental labyrinth. Mice lacking FLRT2 in endothelial cells exhibited embryonic lethality at mid-gestation, with systemic congestion and hypoxia. Although they lacked apparent deformities in the embryonic vasculature and heart, the placental labyrinths of these embryos exhibited aberrant alignment of endothelial cells, which disturbed the feto-maternal circulation. Interestingly, this vascular deformity was related to endothelial repulsion through binding to the UNC5B receptor. Our results suggest that the proper organization of the placental labyrinth depends on coordinated inter-endothelial repulsion, which prevents uncontrolled layering of the endothelium.

KEY WORDS: Angiogenesis, Placenta, Neurovascular, FLRT2, UNC5B

[1]Department of Vascular Biology, The Sakaguchi Laboratory, School of Medicine, Keio University, 35 Shinanomachi, Shinjuku-ku, Tokyo 160-8582, Japan. [2]Department of Surgery, School of Medicine, Keio University, 35 Shinanomachi, Shinjuku-ku, Tokyo 160-8582, Japan. [3]Department of Plastic Surgery, School of Medicine, Keio University, 35 Shinanomachi, Shinjuku-ku, Tokyo 160-8582, Japan. [4]Department of Biochemistry, School of Medicine, Keio University, 35 Shinanomachi, Shinjuku-ku, Tokyo 160-8582, Japan. [5]Department of Cardiology, School of Medicine, Keio University, 35 Shinanomachi, Shinjuku-ku, Tokyo 160-8582, Japan. [6]Department of Signal Transduction, Research Institute for Microbial Diseases, Osaka University, 3-1 Yamada-oka, Suita, Osaka 565-0871, Japan. [7]Department of Molecular Physiology, National Cerebral and Cardiovascular Center Research Institute, 5-7-1 Fujishirodai, Suita, Osaka 565-8565, Japan. [8]Departments of Genetics, Pediatrics, and Medicine (Cardiology), Albert Einstein College of Medicine of Yeshiva University, 1301 Morris Park Avenue, Price Center 420, Bronx, NY 10461, USA. [9]Karlsruhe Institute of Technology (KIT), Zoological Institute, Cell- and Neurobiology, Fritz-Haber-Weg 4, Karlsruhe 76131, Germany. [10]Department of Organ and Tissue Anatomy, Hamamatsu University School of Medicine, 1-20-1, Handayama, Higashi-ku, Hamamatsu, Shizuoka 431-3192, Japan. [11]Department Molecules - Signaling - Development, Max Planck Institute of Neurobiology, Am Klopferspitz 18, Martinsried 82152, Germany. [12]Munich Cluster for Systems Neurology (Synergy), Munich 80336, Germany. [13]Department of Medicine, Program in Molecular Medicine, VA Salt Lake City Health Care System, University of Utah, 15 North 2030 East, Salt Lake City, UT 84112, USA. [14]Department of Oncological Sciences, VA Salt Lake City Health Care System, University of Utah, 15 North 2030 East, Salt Lake City, UT 84112, USA. [15]Department of Human Genetics, VA Salt Lake City Health Care System, University of Utah, 15 North 2030 East, Salt Lake City, UT 84112, USA. [16]ARUP Laboratories, VA Salt Lake City Health Care System, University of Utah, 15 North 2030 East, Salt Lake City, UT 84112, USA. [17]Division of Cardiovascular Medicine, Department of Medicine, VA Salt Lake City Health Care System, University of Utah, 15 North 2030 East, Salt Lake City, UT 84112, USA. [18]Department of Cardiology, VA Salt Lake City Health Care System, University of Utah, 15 North 2030 East, Salt Lake City, UT 84112, USA. [19]Key Laboratory for Human Disease Gene Study, Sichuan Academy of Medical Sciences and Sichuan Provincial People's Hospital, Chengdu 610072, China.

*These authors contributed equally to this work

‡Authors for correspondence (ykubo33@a3.keio.jp; yamagish@hama-med.ac.jp)

I.T.-N., 0000-0003-1665-719X; Y.Y., 0000-0002-5902-1565; N.N., 0000-0002-0757-9532; Y.K., 0000-0001-6672-4122

Received 27 January 2017; Accepted 26 May 2017

INTRODUCTION

The placenta is an organ that is found primarily in mammals and that connects a developing fetus to the maternal uterine wall. The placental labyrinth is a structure located on the fetal side of the placenta, consisting of two major cellular components: trophoblasts and endothelial cells (Cross et al., 1994). Trophoblasts, which are the post-implantation derivatives of the trophectoderm, line the maternal blood spaces, whereas endothelial cells, which arise from the allantoic mesoderm of the embryo, border the fetal circulation (Downs, 2002). These two juxtaposed layers provide the interface for the bidirectional transfer of gases, nutrients, embryonic metabolic end-products, and other molecules between the embryo and mother. Hence, their proper formation is essential for the development of embryos (Rossant and Cross, 2001). Vascular development consists of three major processes: vasculogenesis, angiogenesis and vascular remodeling. In principle, all three of these processes depend on or are highly affected by signaling by vascular endothelial growth factor (VEGF) and its receptors (Potente et al., 2011). However, the detailed mechanisms surrounding VEGF vary greatly from organ to organ, probably contributing to organ-specific vascular patterning (Adams and Alitalo, 2007). The mechanisms that mediate vascularization of the labyrinth share many of the molecules that are required for embryonic vascular development, including hypoxia-inducible factors and VEGF expressed in trophoblasts (Adelman et al., 2000; Rossant and Cross, 2001; Cross et al., 2003; Hirashima et al., 2003). However, the endothelial machinery that specifically mediates establishment of the placental vasculature is largely unclear.

The nervous and vascular systems have been found to share a number of guidance cues for network formation, including members of the ephrin, netrin, semaphorin and slit families (Adams and Eichmann, 2010; Quaegebeur et al., 2011). Fibronectin leucine-rich transmembrane protein 2 (FLRT2) is a member of the fibronectin leucine-rich transmembrane (FLRT) family of proteins, which act as repulsive ligands of the UNC5 receptor family and as chemorepellents for neurons (Lacy et al., 1999; Yamagishi et al., 2011; Seiradake et al., 2014). Outside of the nervous system, FLRT2 is expressed in the epicardium, and its global knockout leads to reduced thickness of the ventricular myocardium, suggesting a role for FLRT2 in heart morphogenesis

Development (2017) 144, 2392-2401 doi:10.1242/dev.149757

(Müller et al., 2011). However, the importance of FLRT2 as a neurovascular cue and the detailed function of FLRT2 in cardiovascular development are still unclear.

Here, we unexpectedly found that FLRT2 is expressed in endothelial cells specifically in the placental labyrinth. Mice lacking endothelial FLRT2 exhibited aberrant alignment of the placental endothelium, which disturbed feto-maternal circulation and might have been responsible for embryonic lethality at mid-gestation. This vascular deformity was caused by a lack of the endothelial repulsion that results from binding of FLRT2 to UNC5B. Netrin 1 has long been thought to be the functional ligand of UNC5B, with absence of netrin 1/UNC5B signaling being responsible for the vascular defects in UNC5B-deficient mice (Lu et al., 2004; Larrivée et al., 2007). Indeed, proteolytic fragments of netrin 1 bind UNC5B in diabetic endothelial cells and increase vascular permeability (Miloudi et al., 2016). However, in terms of developmental angiogenesis, the situation regarding the role of netrin 1/UNC5B signaling is complex and has been subject to debate; notably, the abnormalities reported for UNC5B-deficient mice are absent in netrin 1 mutants (Serafini et al., 1996; Wilson et al., 2006; Castets and Mehlen, 2010; Yung et al., 2015). Our results suggest that FLRT2 is the predominant ligand that is associated with the role of UNC5B in vascular development and indicate that fine-tuning of vascular morphogenesis by inter-endothelial repulsion contributes crucially to the development of the placental labyrinth.

RESULTS

Endothelial FLRT2 is required for mid-gestation embryonic survival

To elucidate the function of FLRT2 in vascular development, we utilized *Tie2-Cre* mice, classically used to delete genes in endothelial cells. By crossing these mice with indicator mice (*flox-CAT-EGFP*), we observed Tie2-Cre expression in endothelial cells and hematopoietic cells at embryonic day (E) 12.5 (Fig. S1A-C), in agreement with results presented previously (Constien et al., 2001). When *Flrt2-flox* mice were crossed with *Tie2-Cre* mice, the resultant endothelial/hematopoietic-specific *Flrt2* knockout mice (*Tie2-Cre*$^{+}$*Flrt2*$^{flox/flox}$: herein referred to as *Flrt2*$^{\Delta EHC}$) died between E13.5 and E14.5 (Fig. 1A,C). Contrary to this observation, in a previous study, some global *Flrt2* knockout mice survived until weaning (Müller et al., 2011). This discrepancy could be explained by the difference in genetic backgrounds, as the previous study involved 129/C57Bl/6J mice, whereas our experiments were based on pure C57Bl/6J mice.

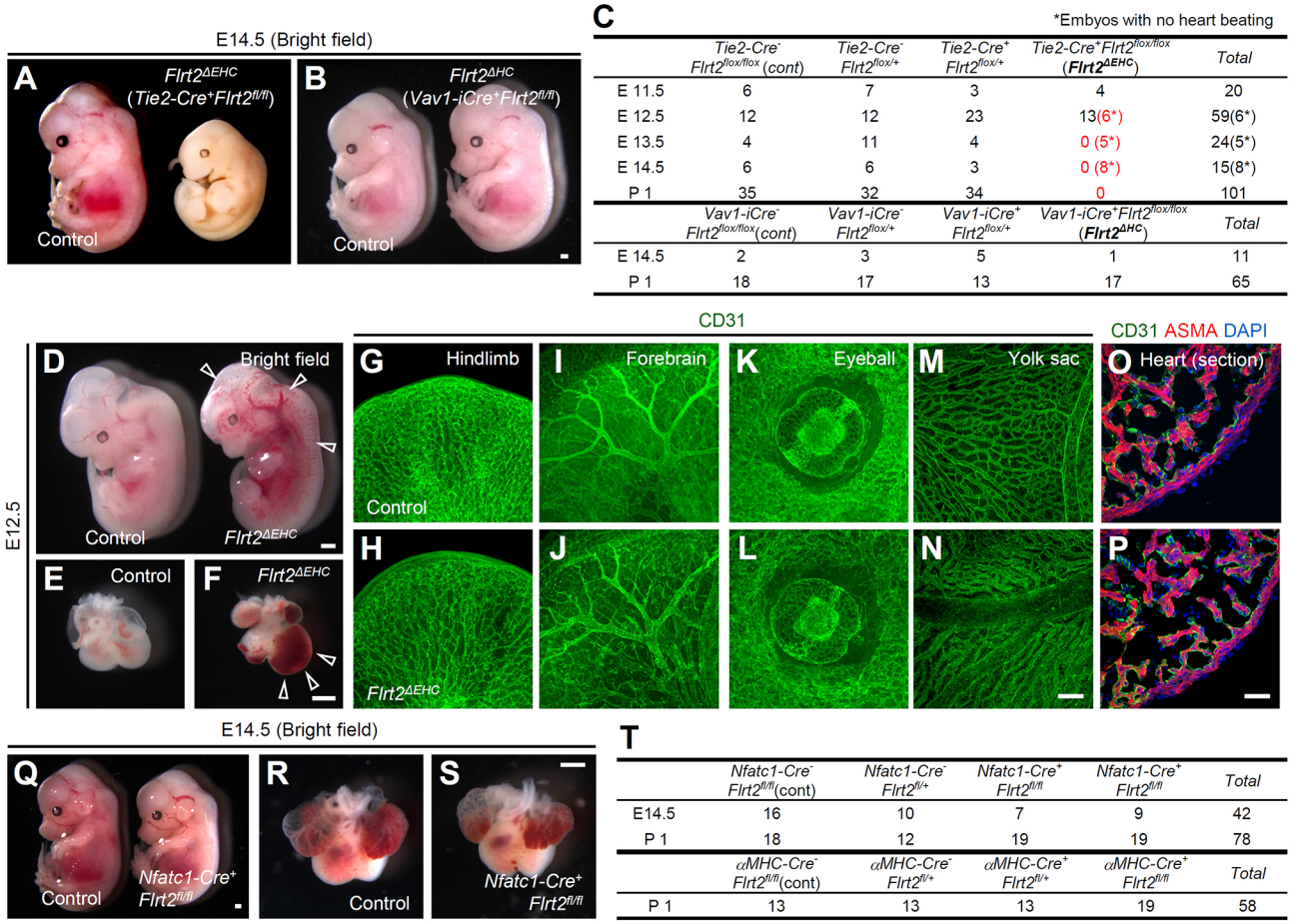

Fig. 1. Endothelial FLRT2 is required for embryonic survival during mid-gestation. (A,B) Bright-field views of embryos with endothelial/hematopoietic-specific *Flrt2* knockout (*Flrt2*$^{\Delta EHC}$) or hematopoietic-specific *Flrt2* knockout (*Flrt2*$^{\Delta HC}$) at E14.5. (C) Genotyping results from the *Flrt2* conditional knockout matings. For *Tie2-Cre* (endothelial/hematopoietic)-specific deletion, a *Tie2-Cre*^{het}*Flrt2*$^{flox/+}$ male was mated with *Flrt2*$^{flox/flox}$ females. For *Vav1-iCre* (hematopoietic)-specific deletion, a *Flrt2*$^{flox/flox}$ male was mated with *Vav1-iCre*^{het}*Flrt2*$^{flox/+}$ females. (D-P) Bright-field views of embryos (D-F), whole-mount tissues stained with CD31 (G-N), or heart sections stained with the indicated antibodies at E12.5 (O,P). Significant congestion (arrowheads) was seen in *Flrt2*$^{\Delta EHC}$ embryos. ASMA, α-smooth muscle actin. (Q-S) Bright-field views of embryos or hearts at E14.5. (T) Genotyping results from the *Flrt2* conditional knockout matings. A *Cre*^{het}*Flrt2*$^{flox/+}$ male was mated with *Flrt2*$^{flox/flox}$ females. Scale bars: 500 µm (A,B,D-F,Q-S); 200 µm (G-N); 50 µm (O,P).

Development (2017) 144, 2392-2401 doi:10.1242/dev.149757

To examine the relevance of hematopoietic FLRT2, we crossed *Flrt2-flox* mice with *Vav1-iCre* mice (de Boer et al., 2003), in which expression of an optimized variant of Cre is expressed in all hematopoietic cells but not in endothelial cells (Fig. S1D-F). The hematopoietic *Flrt2* knockout mice (*Vav1-iCre*$^{+}$*Flrt2*$^{flox/flox}$: herein referred to as *Flrt2*$^{\Delta HC}$) were viable with no detectable abnormalities (Fig. 1B,C).

To explore the cause of embryonic lethality in *Flrt2*$^{\Delta EHC}$ mice, they were examined at earlier stages of development. At E12.5, six out of 13 *Flrt2*$^{\Delta EHC}$ mice had no cardiac rhythm, and the remainder showed systemic congestion (Fig. 1D-F) without any apparent vascular deformities (Fig. 1G-N). However, at E11.5, none of the defects seen at E12.5 was evident (Fig. S1G-K). These data raised the possibility that the lack of FLRT2 in the endocardium of *Flrt2*$^{\Delta EHC}$ mice impaired cardiac morphogenesis and caused heart failure at E12.5 because *Tie2-Cre* is also expressed in the endocardium (Fig. S1L,M). However, morphological and histological examination of the hearts of *Flrt2*$^{\Delta EHC}$ mice showed no apparent structural defects at E12.5 (Fig. 1E,F,O,P). The specific role of FLRT2 in endocardium was examined by crosses with *Nfatc1-Cre* mice (Wu et al., 2012), in which *Cre* is expressed in all endocardial cells, some macrophages, and a few aortic endothelial cells, but not in peripheral endothelial cells (Fig. S1N-Q). The resultant *Flrt2* knockout mice (*Nfatc1-Cre*$^{+}$*Flrt2*$^{flox/flox}$) were viable and showed no detectable abnormalities (Fig. 1Q-T). Moreover, utilizing *αMHC-Cre* mice, we determined that FLRT2 expression in the myocardium is also dispensable for embryonic development (Fig. 1T). Together, these results indicated that endothelial FLRT2 was required for mid-gestation embryonic survival, and that a separate crucial abnormality might exist outside the embryos causing the lethality in *Flrt2*$^{\Delta EHC}$ mice.

FLRT2 is expressed in endothelial cells specifically in the placental labyrinth

The expression pattern of FLRT2 was examined through the generation of *Flrt2*$^{+/lacZ}$ knock-in mice (Fig. S2A,B) and examination of β-galactosidase expression in these mice. In agreement with previously published results, we observed abundant β-galactosidase expression in a population of neurons and the epicardium (Yamagishi et al., 2011; Müller et al., 2011), but not in embryonic endothelial cells (Fig. 2A-C,G,H,K-M). Consistently, in the neonatal retina, we detected β-galactosidase expression in retinal ganglion cells, but not in endothelial cells (Fig. S2C,D), and deletion of *Flrt2* in retinal ganglion cells by the

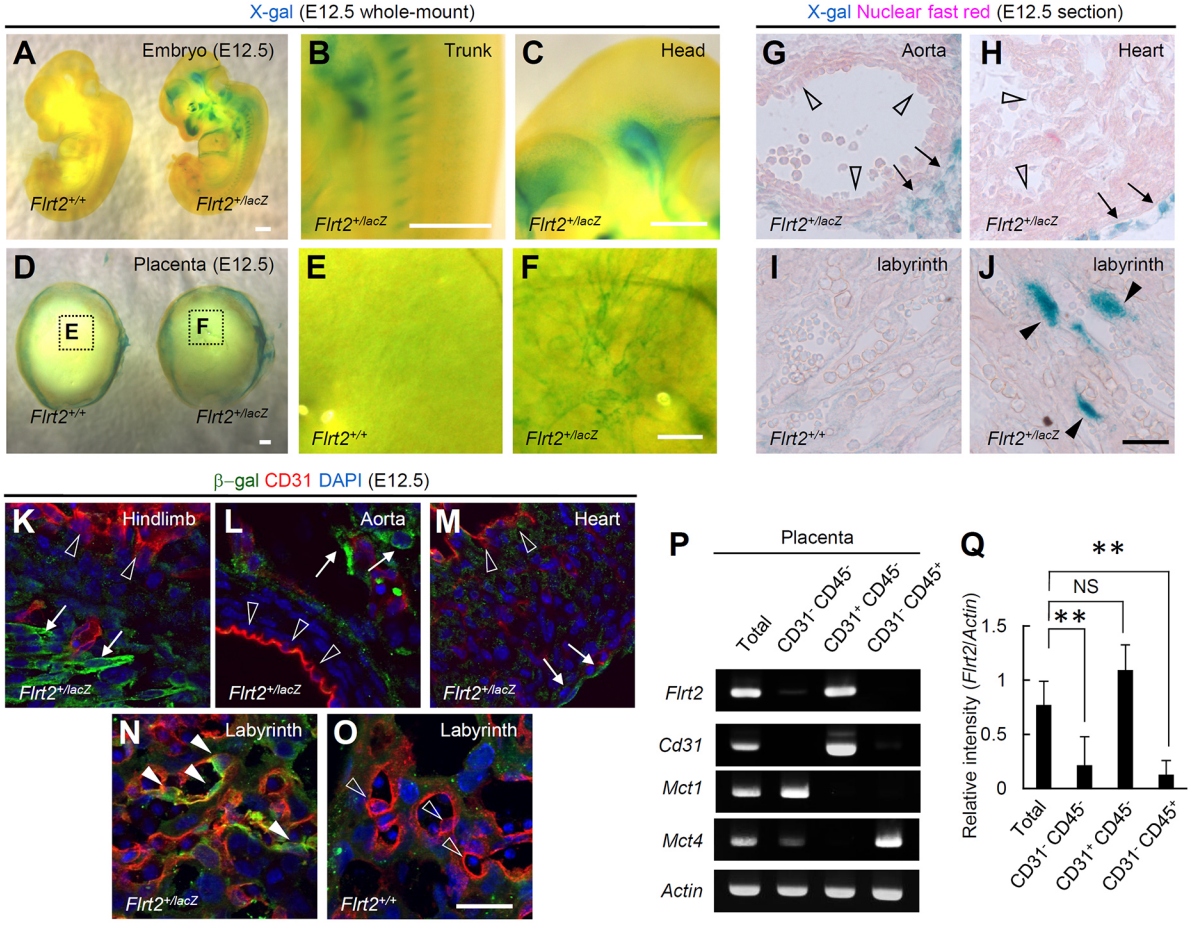

Fig. 2. FLRT2 is specifically expressed in endothelial cells in the placental labyrinth. (A-J) X-gal staining of whole-mount or section samples at E12.5. In *Flrt2*$^{+/lacZ}$ mice, β-galactosidase expression was detected in epicardial and some mesenchymal cells (arrows in G,H) and some placental endothelial cells (filled arrowheads in J), but not in other endothelial cells, including the endocardium and the aortic endothelium (unfilled arrowheads in G,H). (K-O) Immunohistochemistry of placental sections taken at E12.5. *Flrt2*$^{+/lacZ}$ embryos show β-galactosidase activity in some neuronal, stromal or epicardial cells (arrows in K-M), but not in endothelial cells (unfilled arrowheads in K-M). Endothelial β-galactosidase activity was mosaically detected in the placentas of *Flrt2*$^{+/lacZ}$ mice (filled arrowheads in N), but not in those of *Flrt2*$^{+/+}$ mice (unfilled arrowheads in O). (P,Q) RT-PCR analysis and quantification of FACS-sorted cells derived from E12.5 placentas (n=5). *Actb* (Actin) was used as loading control. Scale bars: 500 µm (A-D); 200 µm (E,F); 20 µm (G-O). **P<0.01; NS, not significant. Data are presented as mean±s.d.

Development (2017) 144, 2392-2401 doi:10.1242/dev.149757

use of *Chx10-Cre* mice did not impair retinal vascularization (Fig. S2E-G). It has previously been suggested (but not shown directly) that FLRT2 is expressed in the placental endothelium (Müller et al., 2011). Placental expression was therefore examined in our *Flrt2*$^{+/lacZ}$ knock-in mice, which had a mosaic pattern of β-galactosidase expression in endothelial cells of the placental labyrinth (Fig. 2D-F,I,J,N,O). Immunohistochemistry with anti-FLRT2 antibodies detected patchy expression localized around endothelial cells in the placental labyrinth (Fig. S3A-C). This endothelial FLRT2 immunoreactivity was diminished in *Flrt2*$^{\Delta EHC}$ but not in *Flrt2*$^{\Delta HC}$ mice (Fig. S3D-I), confirming the specificity of the antibodies. Reverse transcription polymerase chain reaction (RT-PCR) analysis of cells sorted by fluorescence-activated cell sorting (FACS) (Fig. S4) confirmed that *Flrt2* expression was enriched in CD31 (PECAM1)$^{+}$ CD45 (PTPRC)$^{-}$ endothelial cells in the placenta (Fig. 2P,Q). Moreover, *Flrt2* expression was elevated in placental CD31^{+} endothelial cells at E12.5 (Fig. S5), suggesting that there is a requirement for endothelial FLRT2 around this developmental stage.

Vasculature is poorly formed and aberrantly organized in FLRT2-deficient placentas

Embryonic death occurring from E10 to E13 is attributed to failures in cardiac function, hematopoiesis or placentation in many cases (Papaioannou and Behringer, 2012). Our observation of the expression of FLRT2 in placental endothelial cells suggested that *Flrt2*$^{\Delta EHC}$ mice might have placental defects, as *Cre* was expressed in placental endothelial cells in *Tie2-Cre* but not in *Vav1-iCre* mice (Fig. S6A,E). Placental *Tie2*-Cre expression was not observed in any trophoblastic-lineage cells marked by CD9 or the monocarboxylate transporters Mct1 (SLC16A1) or Mct4 (SLC16A3) (Fig. S6B-D), was limited to endothelial cells, and was not seen in hematopoietic cells (Fig. S6A), unlike in other tissues (Fig. S1A-C). Histological examination of the placenta revealed that the labyrinth was poorly formed and compact in *Flrt2*$^{\Delta EHC}$ mice at E12.5 (Fig. 3A-F), although the spongiotrophoblast layer was not affected (Fig. S7A-D). Detailed analysis revealed that numbers of nucleated (fetal) erythrocytes, which are normally contained within the endothelial compartment, were considerably lower in *Flrt2*$^{\Delta EHC}$ mice than in controls, whereas non-nucleated (maternal) erythrocytes successfully circulated in the epithelial compartment that was bordered by trophoblasts (Fig. 3G-N,Q). Further analysis of the endothelial structure of *Flrt2*$^{\Delta EHC}$ mice showed that endothelial alignment was aberrant and the endothelium was multi-layered, effectively obstructing the vascular lumen (Fig. 3K-N). Immunohistochemistry with laminin antibodies showed that the basement membrane was invaginating into the endothelial lumen of placentas in *Flrt2*$^{\Delta EHC}$ mice (Fig. 3O,P). The rate of endothelial proliferation did not differ

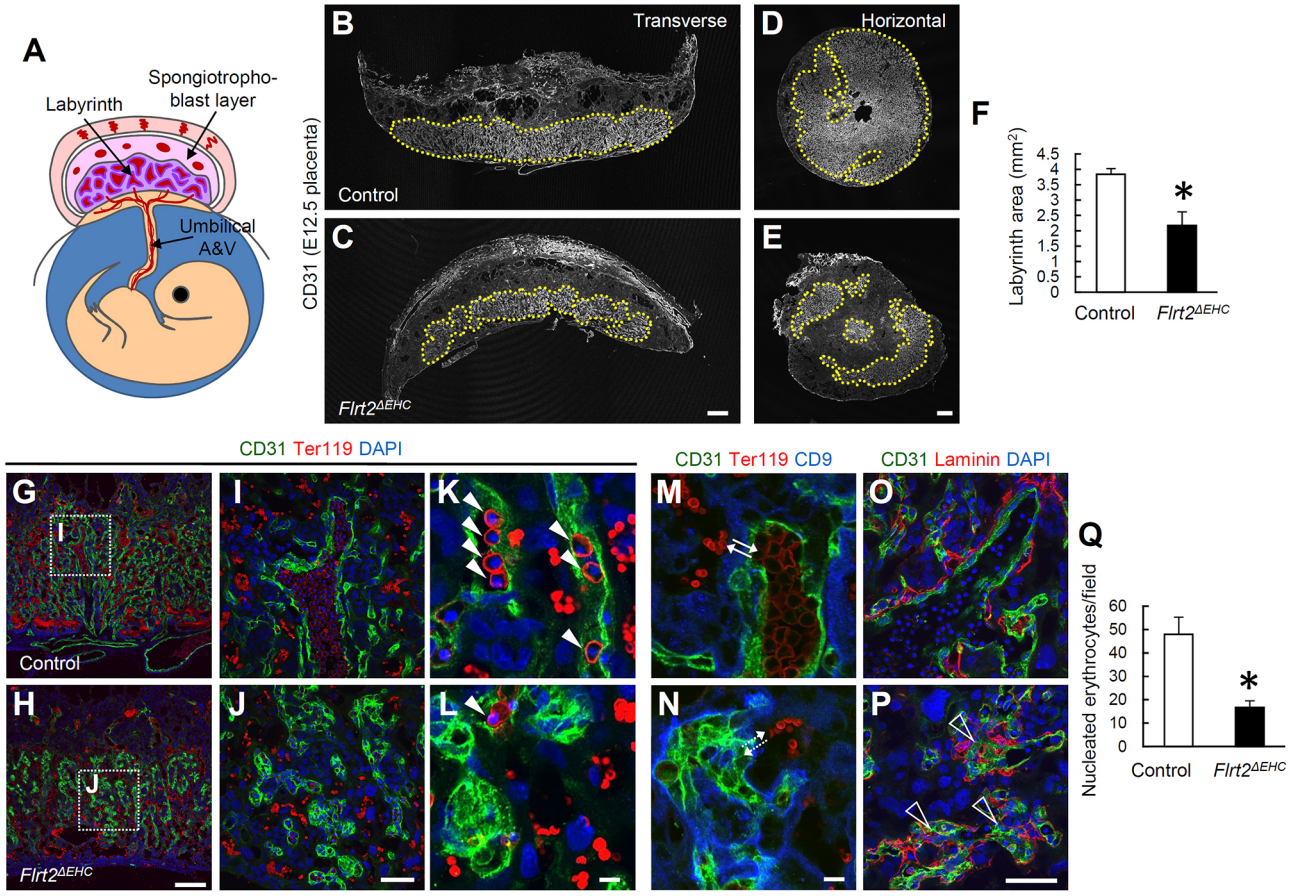

Fig. 3. Poorly formed and aberrantly organized vasculature in FLRT2-deficient placentas. (A) Schematic depicting the anatomy of the mouse placenta. A&V, arteries and veins. (B-Q) Immunohistochemistry and quantification of placental sections at E12.5 (*n*=5). Areas marked by the yellow dotted lines in B-E indicate the placental labyrinth. Filled arrowheads indicate fetal nucleated erythrocytes. The labyrinth in control mice shows intact layering of endothelial cells and trophoblasts between nucleated and non-nucleated erythrocytes (bidirectional arrows in M). The labyrinth of endothelial/hematopoietic-specific *Flrt2* knockout (*Flrt2*$^{\Delta EHC}$) mice shows perturbed layering (dotted bidirectional arrows in N; unfilled arrowheads in P). Scale bars: 500 µm (B-E); 200 µm (G,H); 50 µm (I,J,O,P); 10 µm (K-N). *P<0.05. Data are presented as mean±s.d.

Development (2017) 144, 2392-2401 doi:10.1242/dev.149757

between control and *Flrt2*$^{\Delta EHC}$ mice (Fig. S7E-G), suggesting that the observed endothelial multi-layering could not be attributed to aberrant proliferation.

Increased hypoxia in FLRT2-deficient embryos

The consequences of perturbed feto-maternal gas exchange were explored by examination of the embryos and placentas of *Flrt2*$^{\Delta EHC}$ mice. Bright-field microscopy images suggested that the branches of the umbilical arteries and veins in *Flrt2*$^{\Delta EHC}$ mice were not occluded, but instead contained dark-colored blood (Fig. 4A-C), possibly as a result of impaired gas exchange in the labyrinth. Accumulation of a hypoxia marker, pimonidazole, was significantly higher in *Flrt2*$^{\Delta EHC}$ embryos than in controls, notably in the head region, where oxygen consumption is probably very high (Smith et al., 2013) (Fig. 4D-G).

FLRT2 repulses endothelial cells *in vitro* through the UNC5B receptor

The precise action of FLRT2 on endothelial cells was elucidated with an *in vitro* assay involving primary cultures of endothelial cells. Previously, X-ray crystallography (Seiradake et al., 2014) revealed that FLRT2 binds to FLRT2 (homophilic binding) as well as to UNC5B, UNC5C and UNC5D (heterophilic binding) via different extracellular regions of FLRT2 (Fig. 5A). FLRT2 is known to act as a repulsive cue on neurons through binding to UNC5B and UNC5D (Yamagishi et al., 2011). Among the UNC5 proteins, only UNC5B is indispensable for embryonic development, and *Unc5b* knockouts are lethal at approximately E12.5, similar to the *Flrt2*$^{\Delta EHC}$ genotype (Lu et al., 2004; Navankasattusas et al., 2008). It was, therefore, important to select an endothelial line that expressed both FLRT2 and UNC5B. Human umbilical vein endothelial cells (HUVECs) express these two genes at high levels, making this cell line appropriate for further *in vitro* studies (Fig. 5B). To evaluate whether the repulsive mechanism of interaction between FLRT2 and UNC5B acts in endothelial cells in the same way as in neuronal cells (Yamagishi et al., 2011; Seiradake et al., 2014), a Transwell assay and a stripe assay were performed in HUVECs with recombinant FLRT2 and UNC5B proteins. Compared with vehicle only, FLRT2 significantly decreased migration of HUVECs in the Transwell assay and resulted in repulsion of the cells away from stripes containing the recombinant protein (Fig. 5C-L; Movie 1). These effects were almost completely abolished by neutralization of FLRT2 by the addition of UNC5B, suggesting that the repulsive action of extracellular FLRT2 was mediated by heterophilic interaction with UNC5B, and not by homophilic binding to FLRT2 (Fig. 5C-L). Similar effects were seen with human aortic endothelial cells (HUAECs) (Fig. 5M,N), which express UNC5B but have little or no endogenous expression of FLRT2 (Fig. 5B). Human dermal lymphatic endothelial cells (HDLECs) have little or no UNC5B expression (Fig. 5B), and they did not show repulsion from FLRT2 in stripe assays (Fig. S8A), confirming that the repulsive action of FLRT2 was mediated by UNC5B. To evaluate the role of endogenous UNC5B expression in seeded cells, knockdown of *Unc5b* by small interfering RNA (siRNA) was performed in HUVECs. Treatment with si-Unc5b significantly reduced the repulsive action of FLRT2 on HUVECs (Fig. S8B).

Notably, the effects of FLRT2 on proliferation in HUVECs and HUAECs were negligible (data not shown), suggesting that, *in vitro*, FLRT2 is involved primarily in endothelial repulsion and not in proliferation, which is in agreement with the *in vivo* data in placentas of *Flrt2*$^{\Delta EHC}$ mice (Fig. S7E-G).

Unc5b deletion recapitulates the vascular defects observed in *Flrt2*-deficient placentas

Our results suggested that FLRT2 signals through UNC5B in the placental labyrinth. Endothelial cells in the labyrinth express UNC5B at high levels (Navankasattusas et al., 2008). In *Unc5b*-deficient mice, the results of a previous study with Doppler-flow analysis showed that blood flow is reversed in diastole within the umbilical arteries, suggesting uteroplacental insufficiency (Navankasattusas et al., 2008). Immunohistochemical analysis of histological abnormalities in placentas of *Unc5b*$^{-/-}$ mice showed that the area of the placental labyrinth was significantly reduced at E12.5 compared with *Unc5b*$^{+/+}$ mice (Fig. 6A,B,I), although the spongiotrophoblast layer was not affected (Fig. S9). Similar to our observations in *Flrt2*$^{\Delta EHC}$ mice, placental endothelial alignment was perturbed and fetal circulation was disrupted in *Unc5b*$^{-/-}$ mice (Fig. 6C-H). Taken together, these data suggest that the vascular abnormalities in *Flrt2*$^{\Delta EHC}$ placentas are associated with the repulsive action of FLRT2, acting on the UNC5B receptor on endothelial cells.

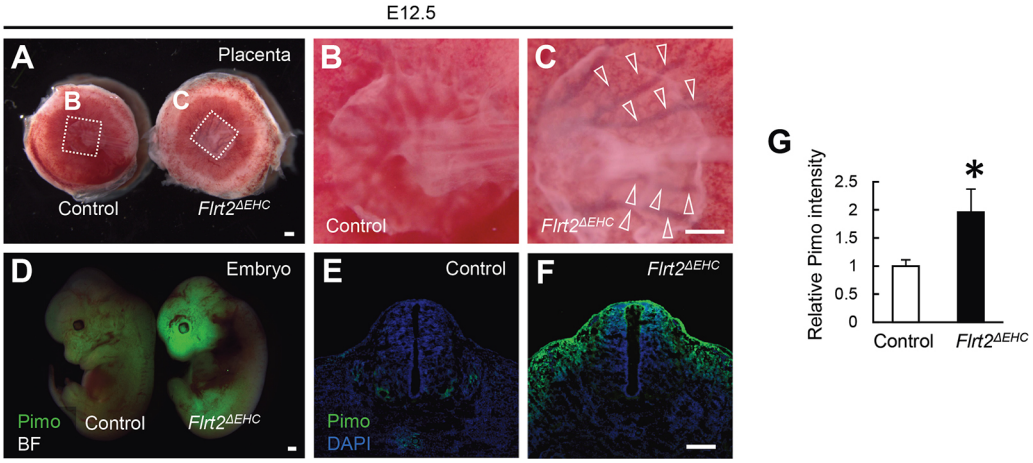

Fig. 4. Increased hypoxia occurs in FLRT2-deficient embryos. (A-C) Bright-field views of placentas at E12.5. Branches of umbilical arteries and veins contain dark-colored blood in endothelial/hematopoietic-specific *Flrt2* knockout (*Flrt2*$^{\Delta EHC}$) mice (arrowheads). (D-G) Whole-mount or sectioned specimens showing pimonidazole incorporation at E12.5 and their quantification (n=5). BF, bright field. Scale bars: 500 µm (A-D); 200 µm (E,F). *P<0.05. Data are presented as mean±s.d.

Development (2017) 144, 2392-2401 doi:10.1242/dev.149757

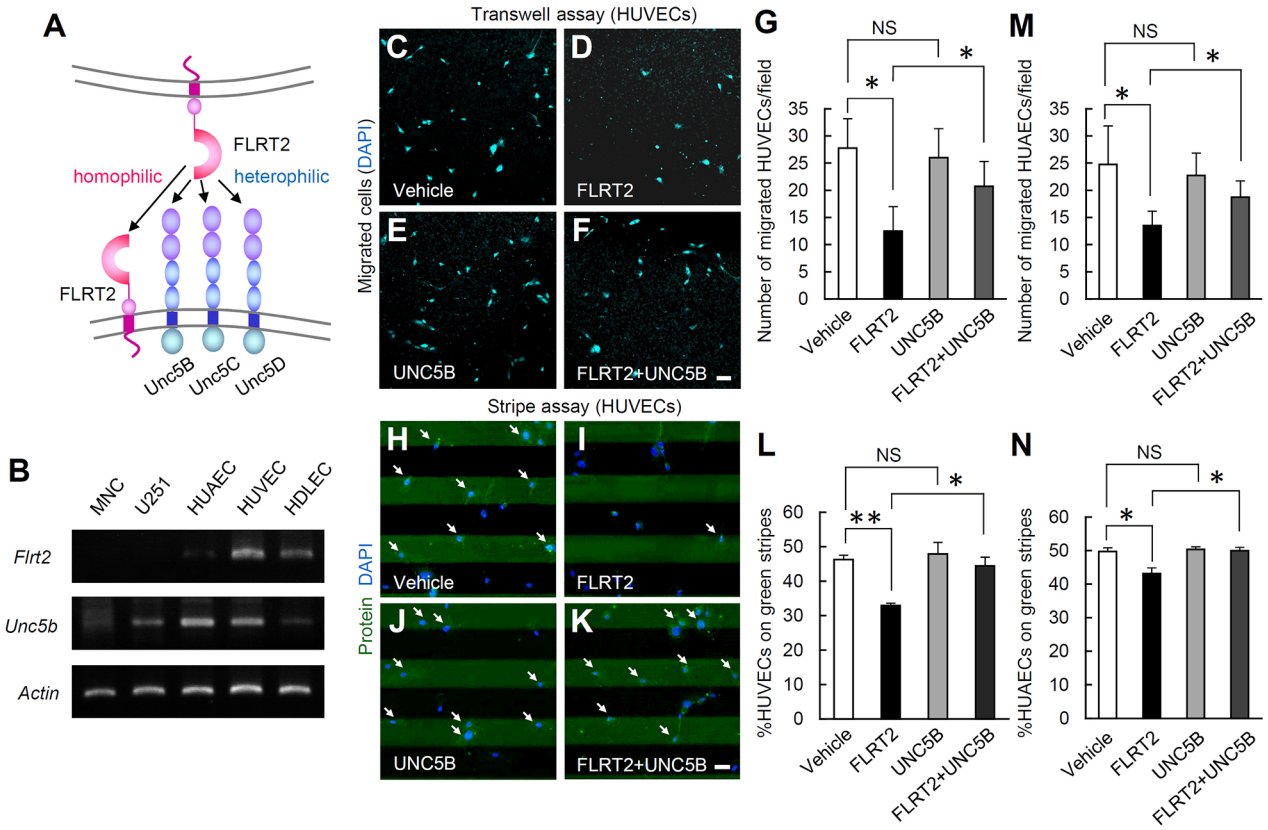

Fig. 5. FLRT2 repulses endothelial cells *in vitro* through the UNC5B receptor. (A) Model showing the FLRT2-FLRT2 and FLRT2-UNC5 interactions. (B) RT-PCR analysis of *FLRT2* and *UNC5B* expression in several different cultured cell types. *ACTB* (Actin) was used as loading control. (C-N) Transwell and stripe assays with HUVECs or HUAECs, and quantification of the results (n=5). Arrows in H-K indicate cells located on the surface where the indicated proteins exist. Scale bars: 50 µm. $^{**}P<0.05$; $^{*}P<0.01$; NS, not significant. Data are presented as mean±s.d.

DISCUSSION

VEGF/VEGF receptor signaling is required for vascular growth during development throughout the body. However, the cellular and molecular mechanisms associated with vascular morphogenesis in each organ vary, and organ-specific angiogenesis involves various VEGF-dependent and VEGF-independent processes. Our results have identified a cellular and molecular mechanism that is specifically active in placental angiogenesis. We have demonstrated that formation of the placental labyrinth requires coordinated inter-endothelial repulsion mediated by FLRT2, which is known to be a repulsive guidance cue for axons, acting via binding to the UNC5B receptor. Our data suggested that, in both $Flrt2^{\Delta EHC}$ mice and $Unc5b^{-/-}$ mice, fetal blood circulation in the placental labyrinth was blocked because of disorganization of vascular structures, impairing feto-maternal gas exchange (Fig. 6J).

The requirement for FLRT2 in development was first demonstrated in whole-body *Flrt2* knockout mice (Müller et al., 2011), in which the thickness of the ventricular walls was severely reduced at E11.5, which is earlier than our observation of placental defects in $Flrt2^{\Delta EHC}$ mice. The phenotype of the whole-body *Flrt2* knockout mice was primarily caused by impaired epicardial integrity, without any endocardial abnormality. In $Flrt2^{\Delta EHC}$ mice, we observed thinning of ventricular walls at E14.5 (data not shown) but not at E12.5, suggesting that placental defects precede cardiac defects in these mice. Overall, the phenotype we observed in $Flrt2^{\Delta EHC}$ mice seems to be independent of the cardiac defects previously observed in global *Flrt2* knockout mice (Müller et al., 2011).

An important aspect of our findings is that they suggest that FLRT2 is the predominant ligand of UNC5B, which explains the severe vascular defects observed in UNC5B-deficient mice (Lu et al., 2004; Navankasattusas et al., 2008). Netrin 1 has long been thought to be the ligand of UNC5B that is involved in angiogenesis. Treatment of endothelial cells with netrin 1 results in tip-cell-filopodia retraction, and this effect is abolished in UNC5B-deficient mice. Morpholino knockdown of *ntn1* (the gene encoding netrin 1) in zebrafish has demonstrated the repulsive guidance activity of netrin 1 for endothelial cells through UNC5B signaling (Lu et al., 2004). However, *Ntn1* knockout mice survive until birth and have no vascular abnormalities (Yung et al., 2015), indicating that netrin 1 is not necessarily the only ligand for UNC5B, and an absence of netrin 1 might be compensated for by other ligands *in vivo*, specifically roundabout homolog 4 or netrin 4 (Koch et al., 2011; Lejmi et al., 2008; Li et al., 2012). Conflicting reports exist regarding the role of netrin 1 as either a pro-angiogenic or anti-angiogenic factor (Lu et al., 2004; Larrivée et al., 2007; Wilson et al., 2006; Castets and Mehlen, 2010). One argument that appears to resolve this dilemma is the ability of netrin 1 to block apoptosis that would otherwise be induced by unbound UNC5B receptors, thus promoting the survival of endothelial cells during angiogenesis (Castets et al., 2009).

Vascular repulsive cues are usually provided by non-endothelial cells around blood vessels. For example, semaphorin 3E, which is secreted by retinal neurons, binds plexin D1-expressing endothelial tip cells and represses their ability to project filopodia (Kim et al., 2011). Notably, consequences of the loss of semaphorin 3E or

Development (2017) 144, 2392-2401 doi:10.1242/dev.149757

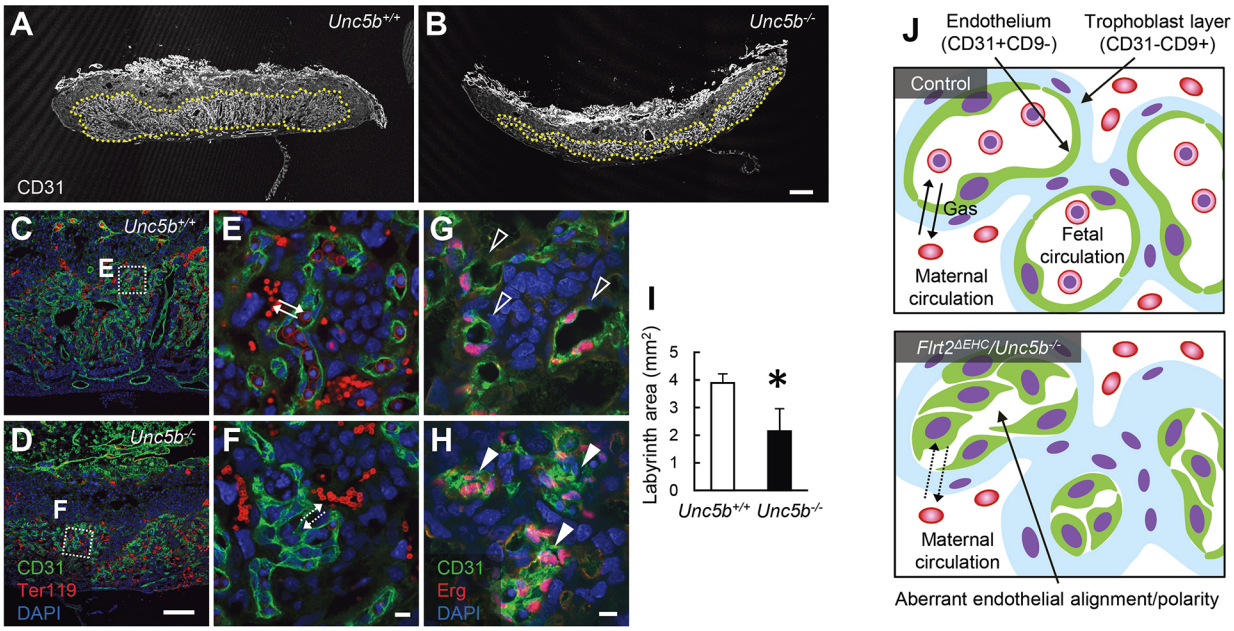

Fig. 6. UNC5B deletion recapitulates the vascular defects observed in *Flrt2*-deficient placentas. (A-I) Immunohistochemistry and quantification of placental sections taken at E12.5 (n=5). The yellow dotted lines in A,B encircle the placental labyrinth. Intact layering of endothelial cells between nucleated and non-nucleated erythrocytes was visible in *Unc5b*$^{+/+}$ placentas (bidirectional arrows in E, unfilled arrowheads in G), but was disrupted in *Unc5b*$^{-/-}$ placentas (dotted bidirectional arrows in F, filled arrowheads in H). (J) Schematic depicting the labyrinth structures of placentas of control, endothelial/hematopoietic-specific *Flrt2* knockout (*Flrt2*$^{\Delta EHC}$), and *Unc5b*$^{-/-}$ mice. Scale bars: 500 µm (A,B); 200 µm (C,D); 10 µm (E-H). *P<0.05. Data are presented as mean±s.d.

plexin D1 are unevenness of the growing front and reduction in branching of the vascular network. Our results also provide evidence that a lack of proper endothelial repulsion results in an overall reduction in vascular growth. Endothelial cell-derived semaphorin 3A has been shown to repel filopodia projection by endothelial tip cells through plexin A1 and neuropilin 1 receptors (Ochsenbein et al., 2016). In agreement with this result, in our model endothelial FLRT2 acts on neighboring UNC5B-expressing endothelial cells to fine-tune alignment and prevent aberrant layering. Upon disruption of FLRT2/UNC5B signaling, endothelial clustering without a change in cell number might lead to failure to expand the total area of vascular plexus.

In contrast to the mosaic pattern of expression of FLRT2 that we observed in endothelial cells, UNC5B has previously been ubiquitously detected in all placental endothelial cells (Navankasattusas et al., 2008). Transmembrane FLRT2 proteins are proteolytically cleaved to release soluble ectodomains (Seiradake et al., 2014; Yamagishi et al., 2011) that diffuse into the extracellular spaces. Thus, it is likely that one FLRT2-expressing endothelial cell acts repulsively on multiple UNC5B-expressing cells, both in paracrine and autocrine manners. Our results indicated that the luminal/abluminal polarity was somehow disrupted in the *Flrt2*$^{\Delta EHC}$ mice, as the basement membrane was invaginating into the endothelial lumen. At the same time, endothelial cells were abnormally clustered, suggesting their impaired alignment or deregulated migration. To evaluate these kinetic components (polarity, alignment and migration) individually will require *in vivo* live imaging, which could not be applied to the mouse placenta with technology available at the time of this study. Although we could not clearly separate the defects in alignment, polarity and migration, the results of our *in vitro* studies suggest that the defects in *Flrt2*$^{\Delta EHC}$ mice involve a mixture of these factors. Endothelial collapse, which is another potential cause of this kind of endothelial clustering, was not apparent, as indicated by the presence of the apoptotic marker cleaved caspase 3 in very few endothelial cells; also, the number of such apoptotic endothelial cells was equal in placentas of control and *Flrt2*$^{\Delta EHC}$ mice (data not shown).

Finally, our data have demonstrated that a FLRT2-UNC5B interaction, resulting in inter-endothelial repulsion, is required for the proper organization of endothelial structures in the placental labyrinth. It will be of interest to explore the roles of similar repellent mechanisms directed by other guidance molecules in the development of other vascular beds. Furthermore, it will be essential to determine whether FLRT2 contributes to adult angiogenesis, in particular angiogenesis associated with certain neoplasms, as tumor angiogenesis often utilizes developmentally important angiogenic molecules (Kubota, 2012).

MATERIALS AND METHODS

Mice and analysis

Animal care was performed in accordance with the Guidelines of Keio University for Animal and Recombinant DNA experiments. The *Tie2-Cre* (Arita et al., 2014), *Chx10-Cre* (Muranishi et al., 2011; Yoshikawa et al., 2016), *Unc5b*$^{-/-}$ (Wilson et al., 2006), *Nfatc1-Cre* (Wu et al., 2012), *αMHC-Cre* (Agah et al., 1997) and *flox-CAT-EGFP* (Kawamoto et al., 2000) mice have been described previously. *Vav1-iCre* mice (de Boer et al., 2003) were obtained from the Jackson Laboratory. An embryonic stem cell clone [*Flrt2*$^{tm1a(EUCOMM)Wtsi}$] obtained from the European Conditional Mouse Mutagenesis Program (EUCOMM) was used to generate *Flrt2-flox* mice. To generate *Flrt2*$^{+/lacZ}$ mice, the *Flrt2* knock-in allele was generated by homologous recombination of exon 2, replaced by a *lacZ* gene followed by a loxP-flanked *PGK*-promoter-driven neomycin gene. *Flrt2*$^{+/lacZ}$ mice were maintained on a CD1 background, and the rest of the mutant mice were crossed with C57BL/6J mice at least ten times. For *Vav1-iCre*-specific deletion, a *Flrt2*$^{flox/flox}$ male was mated with *Vav1-iCre*^{het}*Flrt2*$^{flox/+}$ females. Otherwise, a *Cre*^{het}*Flrt2*$^{flox/+}$ male was mated with *Flrt2*$^{flox/flox}$ females. For analysis, embryos and neonates of both sexes were used without exact determination.

Development (2017) 144, 2392-2401 doi:10.1242/dev.149757

Preparation of tissue sections

Surgically dissected tissues were fixed overnight in 4% paraformaldehyde (PFA) in PBS, and then snap-frozen in optimal cutting temperature (OCT) compound (Sakura Finetechnical, Tokyo, Japan). All placental specimens were sectioned (10-15 µm thick) at the plane where umbilical arteries and veins were attached.

Preparation of whole-mount tissues

Enucleated eyes were fixed for 20 min in 4% PFA in PBS and then dissected as described previously (Okabe et al., 2014). Retinal cups were post-fixed for 20 min. Other tissues were dissected out from embryos and fixed overnight in 4% PFA in PBS. All whole-mount tissues were stained as described below.

Immunostaining

IHC of whole-mount samples or tissue sections was performed as described previously (Kubota et al., 2011). The primary monoclonal antibodies used were hamster anti-CD31 (Chemicon, MAB1398Z; 1:1000), Cy3-conjugated mouse anti-α-smooth muscle actin (Sigma-Aldrich, C6198; 1:500), rat anti-Ter119 (also known as LY76) (R&D Systems, MAB1125; 1:1000), rabbit anti-CD9 (Abcam, ab92726; 1:500) and rat anti-F4/80 (also known as ADGRE1) (Serotech, MCA497R; 1:500). The primary polyclonal antibodies used were Alexa Fluor 488-conjugated rabbit anti-GFP (Molecular Probes, A21311; 1:500), goat anti-GFP (Rockland, 600-101-215; 1:2000), rabbit anti-laminin (Sigma-Aldrich, L9393; 1:500), rabbit anti-ERG (Abcam, ab92513; 1:2000), rabbit anti-β-galactosidase (Millipore, AB986; 1:500), chicken anti-Mct1 (Millipore, AB1286-I; 1:200), rabbit anti-Mct4 (Millipore, AB3314P; 1:200), goat anti-FLRT2 (R&D Systems, AF2877; 1:1000), and rabbit anti-trophoblast specific protein alpha (Tspα; also known as TPBPA) (Abcam, ab104401; 1:1000). Secondary antibodies used were Alexa Fluor 488-conjugated IgGs (Molecular Probes, A11034, A11006, A11055; 1:500) or Cy3/Cy5-DyLight549/DyeLight649-conjugated IgGs (Jackson ImmunoResearch, 711-165-152, 112-165-167, 127-165-160, 711-605-152, 112-605-167, 127-605-160; 1:500). For the 5-ethynyl-2'-deoxyuridine (EdU) incorporation assay, the Click-iT EdU Alexa Fluor 488 Imaging Kit (Invitrogen, C10337) was used. In brief, pregnant mice were injected intraperitoneally 2 h before euthanasia with 0.5 ml EdU solution (0.5 mg ml^{-1}) and stained according to the manufacturer's protocol. For the detection of hypoxic cells, the Hypoxyprobe-1 Plus Kit (Chemicon, HP2-100) was used according to the manufacturer's instructions. In brief, 60 mg kg^{-1} pimonidazole was injected intraperitoneally into pregnant mice 30 min before euthanasia, and sections were stained with Hypoxyprobe Mab1-FITC. For nuclear staining, specimens were treated with 4′,6-diamidino-2-phenylindole (DAPI) (Molecular Probes, D-1306).

X-gal staining of tissue whole-mount samples and sections

Embryos, retinas and placentas were fixed for 30 min in 1% glutaraldehyde in PBS and stained as whole-mount samples or snap-frozen in OCT compound before sectioning. The samples were then incubated for 2 h for whole mounts or 1 h for sections at 37°C with 1 mg ml^{-1} 5-bromo-4-chloro-3-indolyl-β-D-galactopyranoside (X-gal) in a standard X-gal reaction buffer (35 mM potassium ferrocyanide, 35 mmol l^{-1} potassium ferricyanide, 2 mmol l^{-1} $MgCl_2$, 0.02% NP-40 and 0.01% sodium deoxycholate in PBS). For whole-mount embryos and placentas, stained tissues were clarified by immersion in a solution of benzyl alcohol and benzyl benzoate (1:2). For sectioned specimens, Nuclear Fast Red (Thermo Fisher Scientific) was used for counter-staining.

Confocal microscopy

Fluorescent images were obtained using a confocal laser scanning microscope (FV1000; Olympus, Tokyo, Japan). Quantification of cells or parameters of interest was conducted in a 600×600 µm field of view (for all *in vitro* assays), a 200×200 µm field of view (for counting EdU^+ cells) or the entire section (for measuring radial growth and the labyrinth area) in scanned images. ImageJ software (NIH, Bethesda, MD, USA) was used for the quantification of indicated areas in scanned images.

Flow cytometric analysis and cell sorting

Placental tissues were incubated for 20 min at 37°C in Dulbecco's Modified Eagle's Medium (DMEM) containing 1 mg ml^{-1} collagenase IV from *Clostridium histolyticum* (Sigma-Aldrich), 1 U ml^{-1} Dispase (Thermo Fisher Scientific) and 1 U ml^{-1} DNase (Takara-Bio), before cells were dissociated by gentle trituration. Dissociated single cells were preincubated with Fc block (Becton Dickinson) to avoid nonspecific binding of antibodies, and then incubated with allophycocyanin (APC)-conjugated anti-CD31 (Biolegend, 102510; 1:500) and APC-Cy7-conjugated anti-CD45 (Biolegend, 103116; 1:500). Stained samples were analyzed and sorted by SORP FACSAria (Becton Dickinson) with FlowJo software (TreeStar, Ashland, OR, USA), as described previously (Kubota et al., 2011). Debris and dead cells were excluded by forward and side scatter and a negative gate for propidium iodide staining (Fig. S4). FACS studies routinely included unstained control samples and compensation tubes for APC and APC-Cy7. With these negative and positive control tubes, fluorescence voltages and the compensation matrix were set according to the manufacturer's instructions and applied to all the samples that were analyzed.

RT-PCR analysis

Total RNA was prepared from placental tissues or cultured cells, and reverse transcription was performed using Superscript II (Invitrogen). cDNA samples were then subjected to PCR amplification with the following primers: (1) mouse Flrt2, 5′-AGACAAGGCTGCCAGATTACA-3′ and 5′-TAAAATGCAACGTGATGGGG-3′; (2) mouse Cd31, 5′-GCTGAGGA-AAACTCCTTCAC-3′ and 5′-TTCTGGATGGTGAAGTTGGC-3′; (3) mouse Mct1, 5′-ATTGGAGGGCCAGTGGGATA-3′ and 5′-TCAGA-CAGGGCTCTCCTCCT-3′; (4) mouse Mct4, 5′-GCTGTGGTGGACGA-GGGT-3′ and 5′-TGGTTTCCGGGGTATGAA-3′; (5) mouse β-actin, 5′-ATGGATGACGATATCGCTGC-3′ and 5′-AGCACTGTGTTGGCATA-GAG-3′; (6) human FLRT2, 5′-GGAGAAGACGCAGCCGTCAG-3′ and 5′-TTGAAGTCCAGAACTCCAGC-3′; (7) human UNC5B, 5′-ACATT-TGGAGTGGCAGCCAG-3′ and 5′-TCGCTTTGGTGGCAAAGTAA-3′; (8) human β-actin, 5′-ATGGATGATGATATCGCCGC-3′ and 5′-TACA-GGTCTTTGCGGATGTC-3′.

Western blotting

Western blot analysis of embryonic tissues was performed as described elsewhere (Okabe et al., 2014). The primary antibodies used were goat anti-FLRT2 (R&D Systems, AF2877; 1:2000), rabbit anti-β-galactosidase (Cappel Laboratories, 08559761; 1:500) and mouse anti-tubulin (Sigma-Aldrich, T5168; 1:2000).

Transwell assay

HUVECs, HUAECs or HDLECs (Takara-Bio) were cultured in EGM-2 medium (Takara-Bio) at 37°C in 20% O_2 following a previously described protocol (Okuno et al., 2012). Chemotaxis was assessed using Transwell polyester-membrane cell-culture inserts (3.0 µm pore, Sigma-Aldrich) according to the method described previously (Kubota et al., 2011). Both the upper and lower surfaces of the membranes were coated with 0.1% gelatin, and 600 µl EGM-2 medium with or without 5 µg ml^{-1} recombinant FLRT2 (Abcam) and/or 5 µg ml^{-1} recombinant human UNC5B (R&D Systems) was added to the lower wells of 24-well plates. Cells were re-suspended in EGM-2, added to the upper wells (1×10^5 cells per well), and incubated for 12 h. Cells were then fixed by 4% PFA in PBS and stained with DAPI. The number of cells attached to the lower surfaces of the membranes were counted by confocal microscopy as described above.

Stripe assay

Stripe assays were performed as described previously (Yamagishi et al., 2011). Briefly, 50 µg ml^{-1} recombinant control and FLRT2 proteins (Abcam) were pre-clustered with FITC-conjugated anti-His antibodies (Abcam; ab1270; 1:20) in PBS for 30 min. For competition assays, pre-clustered FLRT2 proteins were preincubated with 50 µg ml^{-1} recombinant UNC5B proteins (R&D Systems) for 45 min. These protein solutions were injected into matrices (90 µm width) placed on 60 mm dishes (Knöll et al.,

Development (2017) 144, 2392-2401 doi:10.1242/dev.149757

2007). After incubation at 37°C for 30 min, the dishes were washed with PBS and the matrices were carefully removed, resulting in green fluorescent stripes. The stripes were coated with 50 µg ml^{-1} bovine serum albumin as black stripes for 30 min at 37°C and washed three times with PBS. The stripes were further incubated with 20 µg ml^{-1} laminin (Invitrogen) at 37°C for 1 h, and 10,000 HUVECs or HUAECs were cultured at 37°C for 24 h on the stripes. After incubation, cells were fixed with 4% PFA for 20 min and permeated with 0.3% Triton X-100 in PBS for 15 min at room temperature. DAPI was used to visualize the nuclei, and the total numbers of cells on green and black stripes were quantified. To create movies, phase-contrast pictures were obtained every 5 min from 0.5 h to 16 h after plating the cells and merged with images in the fluorescent channel using Biostation (Nikon, Japan). For RNA interference, HUVECs were washed once with OptiMEM (Thermo Fisher Scientific) and transfected with 40 nmol l^{-1} siRNA Duplex (Qiagen) using 6 µl ml^{-1} Lipofectamine RNAiMAX (Invitrogen) in OptiMEM according to the manufacturer's instructions. After 4 h, the transfection medium was removed and complete culture medium was added. Cells were cultured for a further 48 h before applying to the stripe assay. To knock down *Unc5b*, FlexiTube siRNA GS219699 for UNC5B (Qiagen) was used. As a control, a siRNA-negative control duplex oligonucleotide (5′-CUUACGCUGAGUACUUCGATT-3′, 5′-UCGAAGUACUCAGCG-UAAGTT-3′; Sigma) was used.

Statistics

Results are expressed as mean±s.d. The comparisons between the averages of the two groups were evaluated using a two-tailed Student's *t*-test. *P*-values of <0.05 were considered statistically significant.

Competing interests

The authors declare no competing or financial interests.

Author contributions

Conceptualization: S.Y., Y. Kubota; Methodology: S.Y., Y. Kubota; Software: S.Y., Y. Kubota; Validation: I.T.-N., Y.Y., N.N., K. Okabe, S.Y., Y. Kubota; Formal analysis: T.A., K. Okabe, Y.S., S.Y., Y. Kubota; Investigation: I.T.-N., Y.Y., N.N., T.A., Y.S., S.Y., Y. Kubota; Resources: M.I., N.T., O.N., B.Z., M.B., R.K., S.N., D.L., S.Y.; Data curation: Y. Kubota; Writing - original draft: S.N., S.Y., Y. Kubota; Writing - review & editing: K. Okabayashi, Y. Kubota; Visualization: S.Y., Y. Kubota; Supervision: M.S., Y. Kitagawa, K.S., R.K., D.Y.L., S.Y., Y. Kubota; Project administration: Y. Kubota; Funding acquisition: Y. Kubota

Funding

This work was supported by Grants-in-Aid for Specially Promoted Research from the Ministry of Education, Culture, Sports, Science, and Technology of Japan (22122002, 25122707, 25713059, 15K15089), and by research grants from Inamori Foundation, The Kao Foundation for Arts and Sciences, The Uehara Memorial Foundation, Takeda Science Foundation, SENSHIN Medical Research Foundation, and Toray Industries.

Supplementary information

Supplementary information available online at
http://dev.biologists.org/lookup/doi/10.1242/dev.149757.supplemental

References

Adams, R. H. and Alitalo, K. (2007). Molecular regulation of angiogenesis and lymphangiogenesis. *Nat. Rev. Mol. Cell. Biol.* **8**, 464-478.

Adams, R. H. and Eichmann, A. (2010). Axon guidance molecules in vascular patterning. *Cold Spring Harb. Perspect. Biol.* **2**, a001875.

Adelman, D. M., Gertsenstein, M., Nagy, A., Simon, M. C. and Maltepe, E. (2000). Placental cell fates are regulated in vivo by HIF-mediated hypoxia responses. *Genes Dev.* **14**, 3191-3203.

Agah, R., Frenkel, P. A., French, B. A., Michael, L. H., Overbeek, P. A. and Schneider, M. D. (1997). Gene recombination in postmitotic cells. Targeted expression of Cre recombinase provokes cardiac-restricted, site-specific rearrangement in adult ventricular muscle in vivo. *J. Clin. Invest.* **100**, 169-179.

Arita, Y., Nakaoka, Y., Matsunaga, T., Kidoya, H., Yamamizu, K., Arima, Y., Kataoka-Hashimoto, T., Ikeoka, K., Yasui, T., Masaki, T. et al. (2014). Myocardium-derived angiopoietin-1 is essential for coronary vein formation in the developing heart. *Nat. Commun.* **5**, 4552.

Castets, M. and Mehlen, P. (2010). Netrin-1 role in angiogenesis: to be or not to be a pro-angiogenic factor? *Cell Cycle* **9**, 1466-1471.

Castets, M., Coissieux, M.-M., Delloye-Bourgeois, C., Bernard, L., Delcros, J.-G., Bernet, A., Laudet, V. and Mehlen, P. (2009). Inhibition of endothelial cell apoptosis by netrin-1 during angiogenesis. *Dev. Cell.* **16**, 614-620.

Constien, R., Forde, A., Liliensiek, B., Gröne, H.-J., Nawroth, P., Hämmerling, G. and Arnold, B. (2001). Characterization of a novel EGFP reporter mouse to monitor Cre recombination as demonstrated by a Tie2 Cre mouse line. *Genesis* **30**, 36-44.

Cross, J. C., Werb, Z. and Fisher, S. J. (1994). Implantation and the placenta: key pieces of the development puzzle. *Science* **266**, 1508-1518.

Cross, J. C., Simmons, D. G. and Watson, E. D. (2003). Chorioallantoic morphogenesis and formation of the placental villous tree. *Ann. N. Y. Acad. Sci.* **995**, 84-93.

de Boer, J., Williams, A., Skavdis, G., Harker, N., Coles, M., Tolaini, M., Norton, T., Williams, K., Roderick, K., Potocnik, A. J. et al. (2003). Transgenic mice with hematopoietic and lymphoid specific expression of Cre. *Eur. J. Immunol.* **33**, 314-325.

Downs, K. M. (2002). Early placental ontogeny in the mouse. *Placenta* **23**, 116-131.

Hirashima, M., Lu, Y., Byers, L. and Rossant, J. (2003). Trophoblast expression of fms-like tyrosine kinase 1 is not required for the establishment of the maternal-fetal interface in the mouse placenta. *Proc. Natl. Acad. Sci. USA* **100**, 15637-15642.

Kawamoto, S., Niwa, H., Tashiro, F., Sano, S., Kondoh, G., Takeda, J., Tabayashi, K. and Miyazaki, J. (2000). A novel reporter mouse strain that expresses enhanced green fluorescent protein upon Cre-mediated recombination. *FEBS Lett.* **470**, 263-268.

Kim, J., Oh, W.-J., Gaiano, N., Yoshida, Y. and Gu, C. (2011). Semaphorin 3E-Plexin-D1 signaling regulates VEGF function in developmental angiogenesis via a feedback mechanism. *Genes Dev.* **25**, 1399-1411.

Knöll, B., Weinl, C., Nordheim, A. and Bonhoeffer, F. (2007). Stripe assay to examine axonal guidance and cell migration. *Nat. Protoc.* **2**, 1216-1224.

Koch, A. W., Mathivet, T., Larrivée, B., Tong, R. K., Kowalski, J., Pibouin-Fragner, L., Bouvrée, K., Stawicki, S., Nicholes, K., Rathore, N. et al. (2011). Robo4 maintains vessel integrity and inhibits angiogenesis by interacting with UNC5B. *Dev. Cell* **20**, 33-46.

Kubota, Y. (2012). Tumor angiogenesis and anti-angiogenic therapy. *Keio J. Med.* **61**, 47-56.

Kubota, Y., Takubo, K., Hirashima, M., Nagoshi, N., Kishi, K., Okuno, Y., Nakamura-Ishizu, A., Sano, K., Murakami, M., Ema, M. et al. (2011). Isolation and function of mouse tissue resident vascular precursors marked by myelin protein zero. *J. Exp. Med.* **208**, 949-960.

Lacy, S. E., Bönnemann, C. G., Buzney, E. A. and Kunkel, L. M. (1999). Identification of FLRT1, FLRT2, and FLRT3: a novel family of transmembrane leucine-rich repeat proteins. *Genomics* **62**, 417-426.

Larrivée, B., Freitas, C., Trombe, M., Lv, X., DeLafarge, B., Yuan, L., Bouvrée, K., Bréant, C., Del Toro, R., Bréchot, N. et al. (2007). Activation of the UNC5B receptor by Netrin-1 inhibits sprouting angiogenesis. *Genes Dev.* **21**, 2433-2447.

Lejmi, E., Leconte, L., Pédron-Mazoyer, S., Ropert, S., Raoul, W., Lavalette, S., Bouras, I., Feron, J.-G., Maitre-Boube, M., Assayag, F. et al. (2008). Netrin-4 inhibits angiogenesis via binding to neogenin and recruitment of Unc5B. *Proc. Natl. Acad. Sci. USA* **105**, 12491-12496.

Li, Y. N., Pinzón-Duarte, G., Dattilo, M., Claudepierre, T., Koch, M. and Brunken, W. J. (2012). The expression and function of netrin-4 in murine ocular tissues. *Exp. Eye Res.* **96**, 24-35.

Lu, X., Le Noble, F., Yuan, L., Jiang, Q., De Lafarge, B., Sugiyama, D., Bréant, C., Claes, F., De Smet, F., Thomas, J.-L. et al. (2004). The netrin receptor UNC5B mediates guidance events controlling morphogenesis of the vascular system. *Nature* **432**, 179-186.

Miloudi, K., Binet, F., Wilson, A., Cerani, A., Oubaha, M., Menard, C., Henriques, S., Mawambo, G., Dejda, A., Nguyen, P. T. et al. (2016). Truncated netrin-1 contributes to pathological vascular permeability in diabetic retinopathy. *J. Clin. Invest.* **126**, 3006-3022.

Müller, P.-S., Schulz, R., Maretto, S., Costello, I., Srinivas, S., Bikoff, E. and Robertson, E. (2011). The fibronectin leucine-rich repeat transmembrane protein Flrt2 is required in the epicardium to promote heart morphogenesis. *Development* **138**, 1297-1308.

Muranishi, Y., Terada, K., Inoue, T., Katoh, K., Tsujii, T., Sanuki, R., Kurokawa, D., Aizawa, S., Tamaki, Y. and Furukawa, T. (2011). An essential role for RAX homeoprotein and NOTCH-HES signaling in Otx2 expression in embryonic retinal photoreceptor cell fate determination. *J. Neurosci.* **31**, 16792-16807.

Navankasattusas, S., Whitehead, K. J., Suli, A., Sorensen, L. K., Lim, A. H., Zhao, J., Park, K. W., Wythe, J. D., Thomas, K. R., Chien, C.-B. et al. (2008). The netrin receptor UNC5B promotes angiogenesis in specific vascular beds. *Development* **135**, 659-667.

Ochsenbein, A. M., Karaman, S., Proulx, S. T., Berchtold, M., Jurisic, G., Stoeckli, E. T. and Detmar, M. (2016). Endothelial cell-derived semaphorin 3A inhibits filopodia formation by blood vascular tip cells. *Development* **143**, 589-594.

Okabe, K., Kobayashi, S., Yamada, T., Kurihara, T., Tai-Nagara, I., Miyamoto, T., Mukouyama, Y.-S., Sato, T. N., Suda, T., Ema, M. et al. (2014). Neurons limit angiogenesis by titrating VEGF in retina. *Cell* **159**, 584-596.

Development (2017) 144, 2392-2401 doi:10.1242/dev.149757

Okuno, Y., Nakamura-Ishizu, A., Otsu, K., Suda, T. and Kubota, Y. (2012). Pathological neoangiogenesis depends on oxidative stress regulation by ATM. *Nat. Med.* **18**, 1208-1216.

Papaioannou, V. E. and Behringer, R. R. (2012). Early embryonic lethality in genetically engineered mice: diagnosis and phenotypic analysis. *Vet. Pathol.* **49**, 64-70.

Potente, M., Gerhardt, H. and Carmeliet, P. (2011). Basic and therapeutic aspects of angiogenesis. *Cell* **146**, 873-887.

Quaegebeur, A., Lange, C. and Carmeliet, P. (2011). The neurovascular link in health and disease: molecular mechanisms and therapeutic implications. *Neuron* **71**, 406-424.

Rossant, J. and Cross, J. C. (2001). Placental development: lessons from mouse mutants. *Nat. Rev. Genet.* **2**, 538-548.

Seiradake, E., del Toro, D., Nagel, D., Cop, F., Härtl, R., Ruff, T., Seyit-Bremer, G., Harlos, K., Border, E. C., Acker-Palmer, A. et al. (2014). FLRT structure: balancing repulsion and cell adhesion in cortical and vascular development. *Neuron* **84**, 370-385.

Serafini, T., Colamarino, S. A., Leonardo, E. D., Wang, H., Beddington, R., Skarnes, W. C. and Tessier-Lavigne, M. (1996). Netrin-1 is required for commissural axon guidance in the developing vertebrate nervous system. *Cell* **87**, 1001-1014.

Smith, F., Hu, D., Young, N. M., Lainoff, A. J., Jamniczky, H. A., Maltepe, E., Hallgrimsson, B. and Marcucio, R. S. (2013). The effect of hypoxia on facial shape variation and disease phenotypes in chicken embryos. *Dis. Model. Mech.* **6**, 915-924.

Wilson, B. D., Ii, M., Park, K. W., Suli, A., Sorensen, L. K., Larrieu-Lahargue, F., Urness, L. D., Suh, W., Asai, J., Kock, G. A. et al. (2006). Netrins promote developmental and therapeutic angiogenesis. *Science* **313**, 640-644.

Wu, B., Zhang, Z., Lui, W., Chen, X., Wang, Y., Chamberlain, A. A., Moreno-Rodriguez, R. A., Markwald, R. R., O'Rourke, B. P., Sharp, D. J. et al. (2012). Endocardial cells form the coronary arteries by angiogenesis through myocardial-endocardial VEGF signaling. *Cell* **151**, 1083-1096.

Yamagishi, S., Hampel, F., Hata, K., del Toro, D., Schwark, M., Kvachnina, E., Bastmeyer, M., Yamashita, T., Tarabykin, V., Klein, R. et al. (2011). FLRT2 and FLRT3 act as repulsive guidance cues for Unc5-positive neurons. *EMBO J.* **30**, 2920-2933.

Yoshikawa, Y., Yamada, T., Tai-Nagara, I., Okabe, K., Kitagawa, Y., Ema, M. and Kubota, Y. (2016). Developmental regression of hyaloid vasculature is triggered by neurons. *J. Exp. Med.* **213**, 1175-1183.

Yung, A. R., Nishitani, A. M. and Goodrich, L. V. (2015). Phenotypic analysis of mice completely lacking netrin 1. *Development* **142**, 3686-3691.

Supplementary Figures

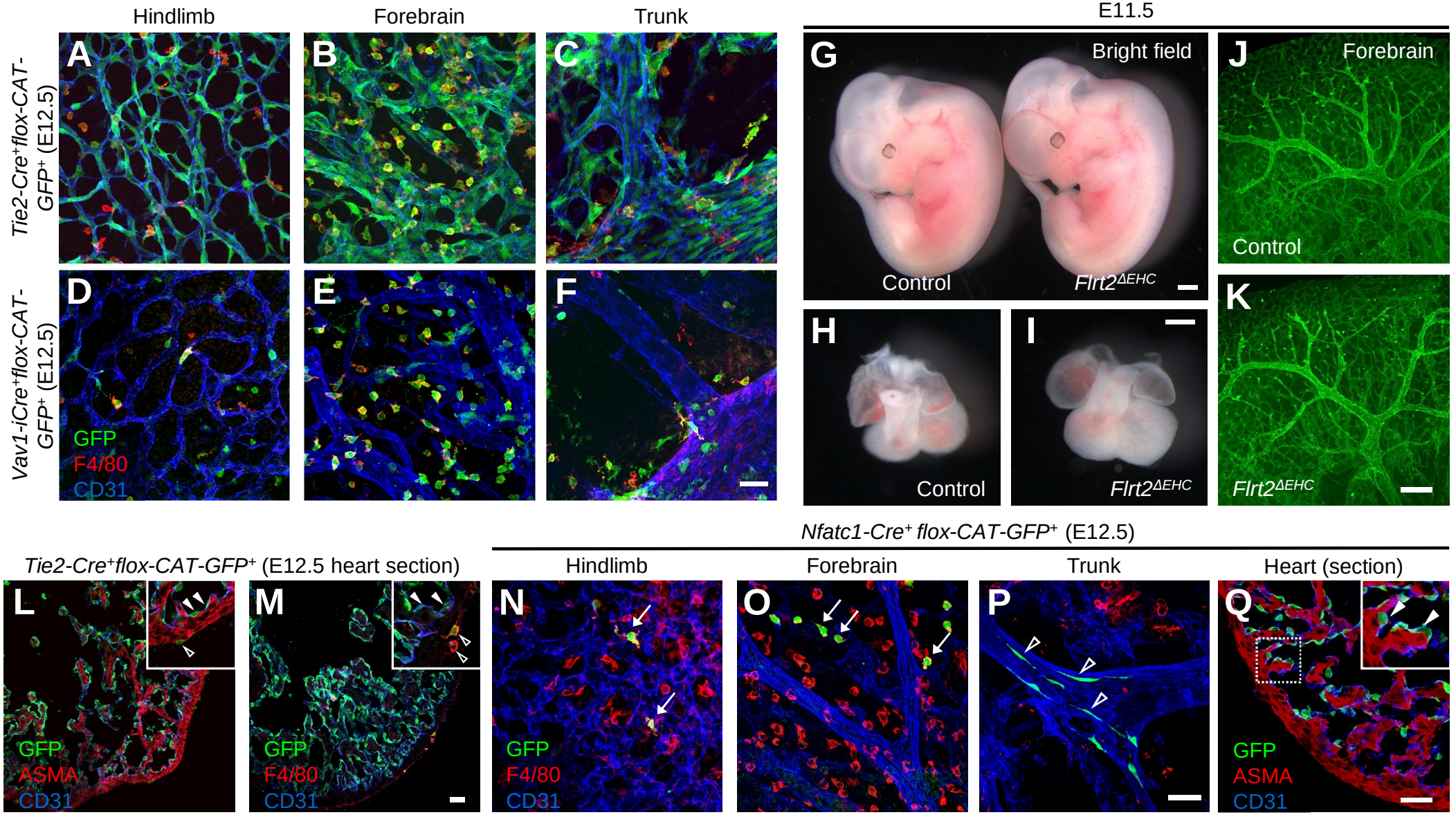

Supplementary Figure 1. Expression patterns of Cre in each Cre line.

(**A–F**) Expression of green fluorescent protein (GFP) was used as a reporter of *Cre* expression. Whole-mount immunostaining of tissues at embryonic day (E)12.5. (**G–K**) Bright-field views of embryos and hearts, or whole-mount tissues stained with CD31 at E11.5. (**L, M**) Heart sections stained with the indicated antibodies at E12.5. GFP was detected in endocardial cells (closed arrowheads) and macrophages (open arrowheads). (**N–Q**) Whole-mount tissues or heart sections at E12.5 stained with the indicated antibodies. GFP was detected in endocardial (closed arrowheads) and some aortic endothelial cells (open arrowheads) and macrophages (arrows). Scale bars: 500 µm (**G–I**); 50 µm (**A–F**, **J–Q**).

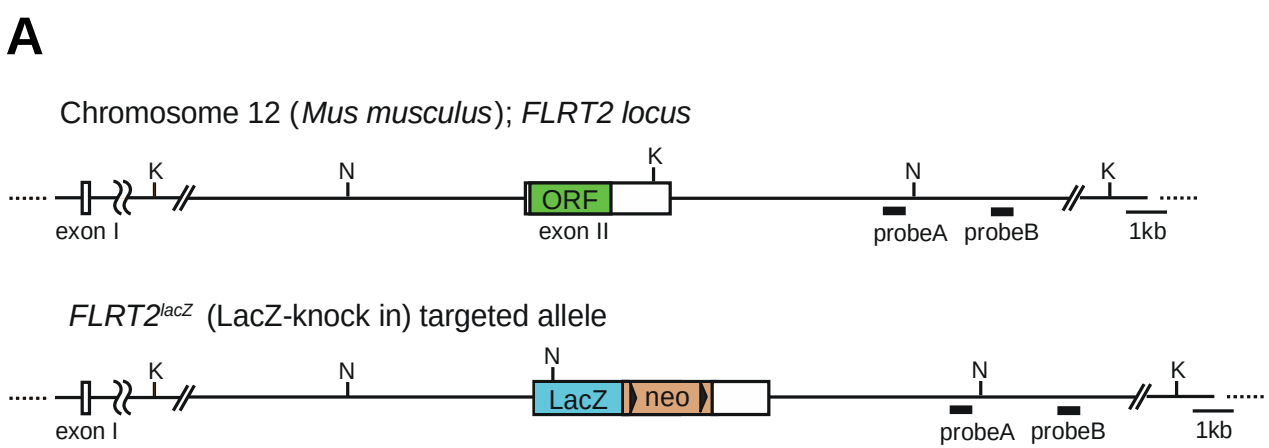

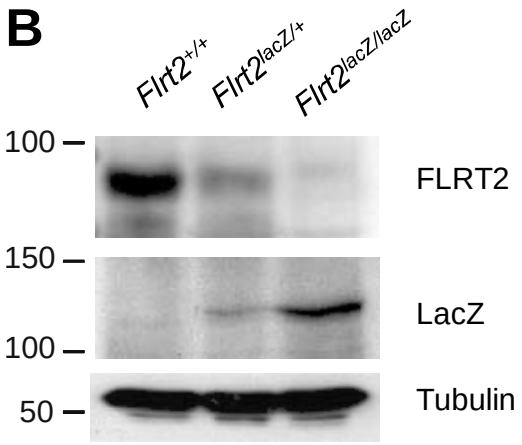

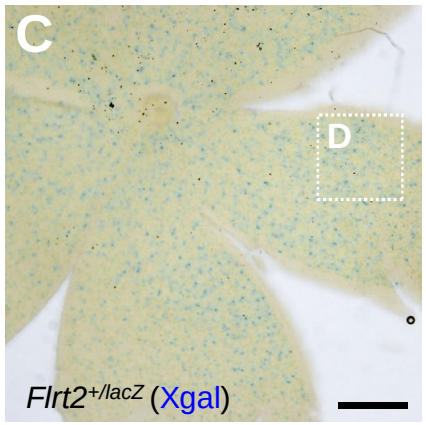

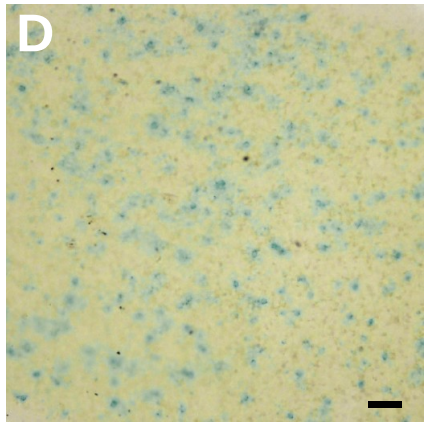

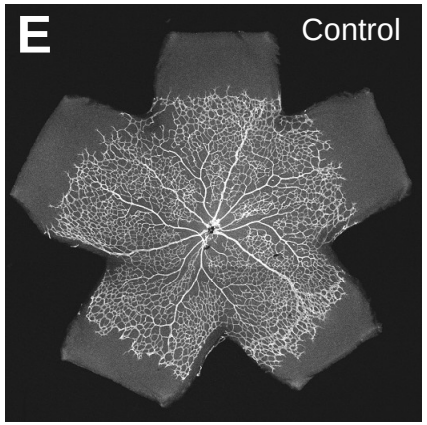

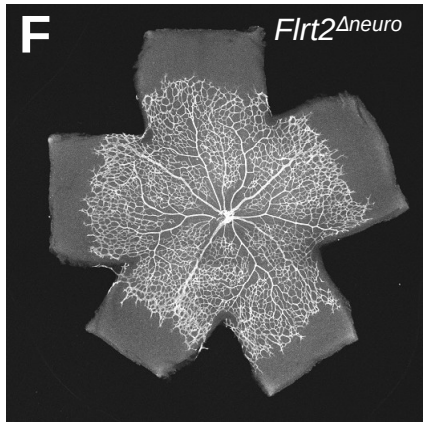

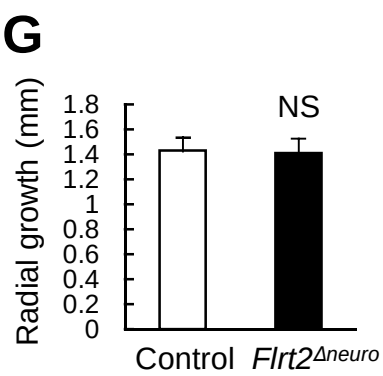

Supplementary Figure 2. Flrt2 is expressed but is dispensable in postnatal retinal neurons.

(**A**) Scheme of the *Flrt2–LacZ* knock-in allele generated by homologous recombination of exon II, containing the entire open reading frame (ORF) of the mouse *Flrt2* gene. Exon II of the *Flrt2* allele was replaced by a *LacZ* gene followed by a loxP-flanked *PGK*-promoter-driven neomycin gene. Recombination in the embryonic stem cell clone was confirmed by Southern blotting using probes A and B. N, NcoI site for probe A; K, Kpn site for probe B. (**B**) Western blot analysis showing FLRT2 and β-galactosidase protein levels. Compared with $Flrt2^{+/+}$, FLRT2 protein levels were lower in heterozygotes and absent in $Flrt2^{lacZ/lacZ}$ mice, whereas β-galactosidase appeared in heterozygotes and was increased in $Flrt2^{lacZ/lacZ}$ mice. Tubulin was used as a loading control. (**C, D**) X-gal staining of whole-mount retinas at P6. (**E–G**) Immunohistochemistry and quantification of P6 retinas stained with CD31 (n = 5). Scale bars: 500 µm (**C, E, F**); 50 µm (**D**). NS, not significant. Data are presented as the mean ± SD.

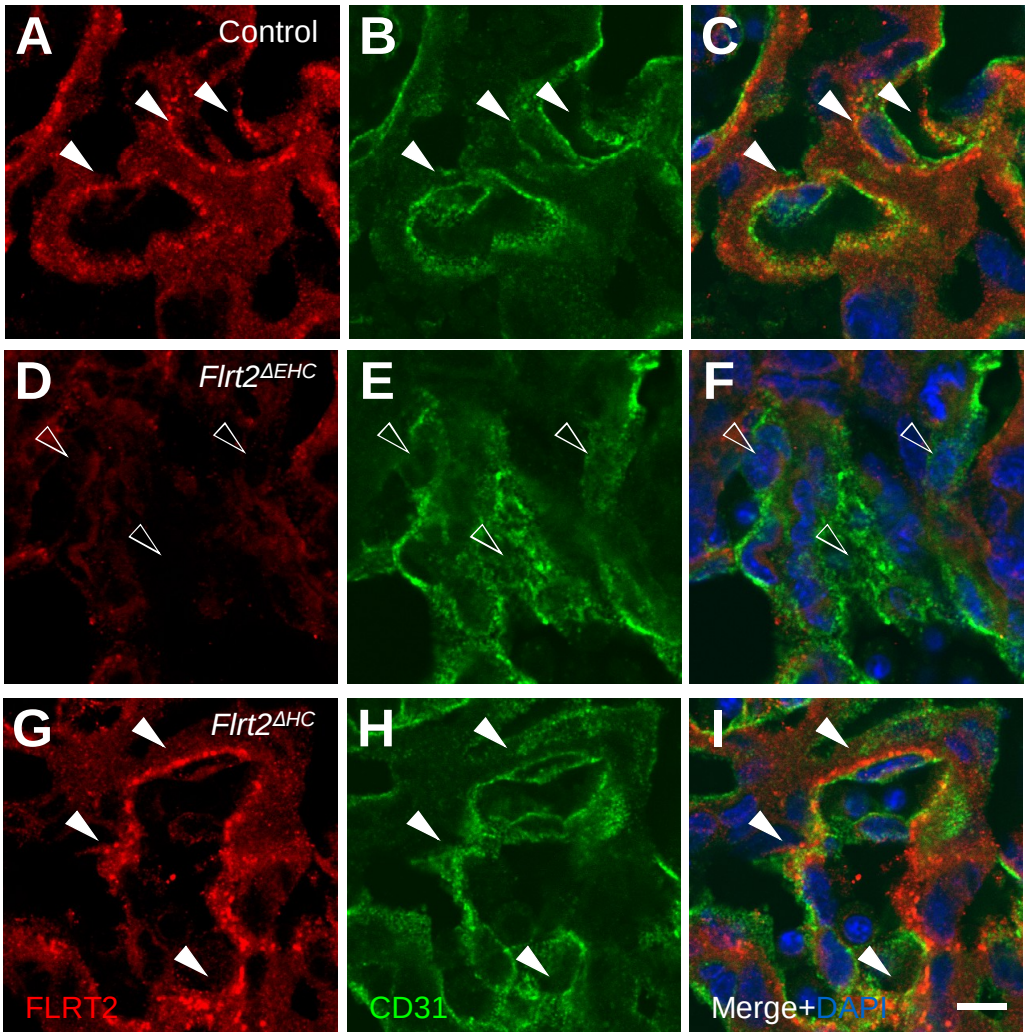

Supplementary Figure 3. FLRT2 protein is detected around placental endothelial cells.

Immunohistochemistry with anti-FLRT2 antibodies on section specimens of placentas at embryonic day (E)12.5. FLRT2 was detected around endothelial cells in control and hematopoietic-specific *Flrt2*-knockout (*Flrt2*$^{\Delta HC}$) mice (closed arrowheads), and this immunoreactivity was diminished in endothelial/hematopoietic-specific *Flrt2*-knockout (*Flrt2*$^{\Delta EHC}$) mice (open arrowheads). Scale bar: 10 µm.

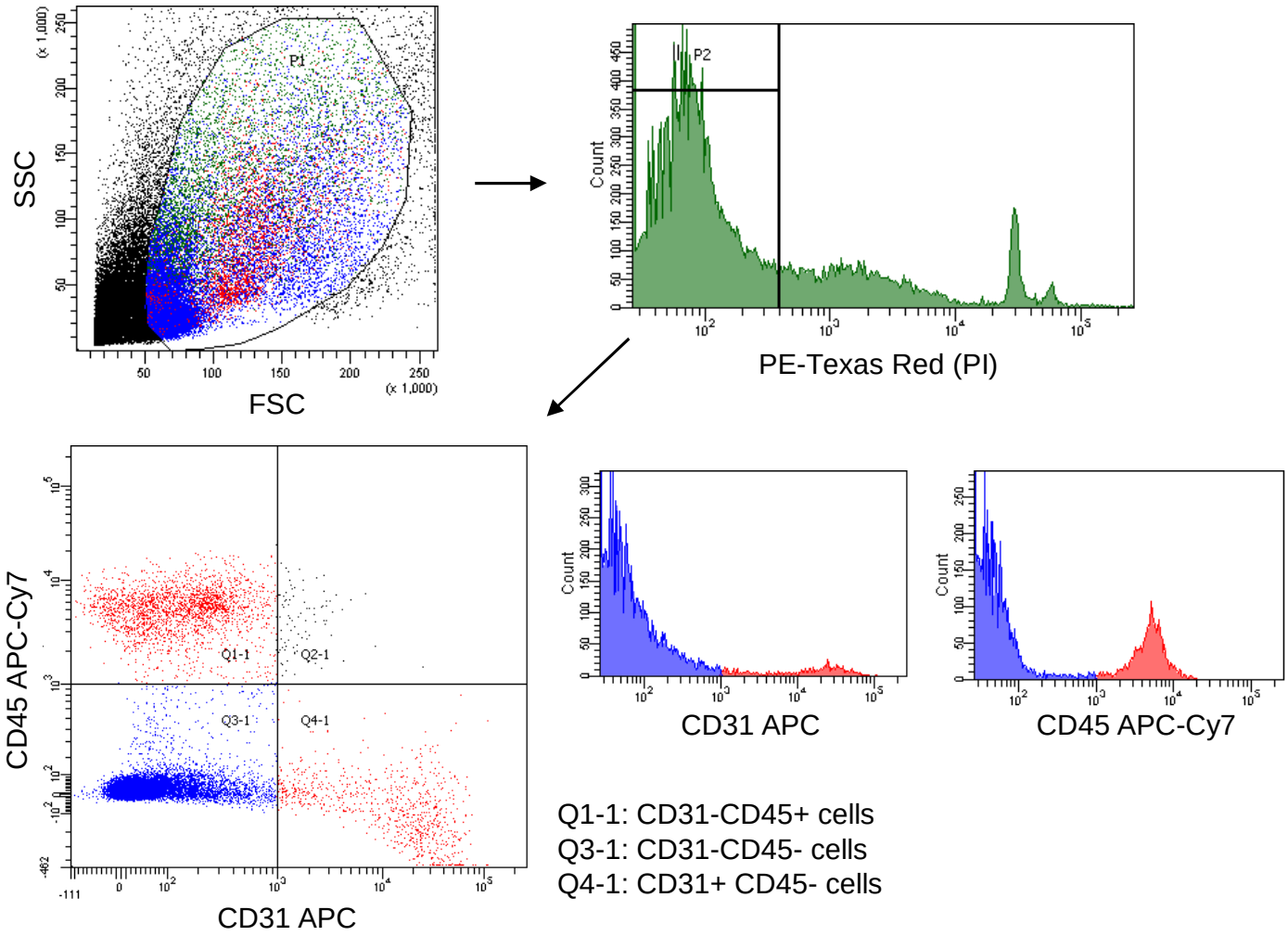

Supplementary Figure 4. Sorting strategy of CD31$^+$ or CD45$^+$ cells from placental tissues.

Stained samples were sorted by SORP FACSAria. Debris and dead cells were excluded by forward and side scatter and a negative gate for propidium iodide staining.

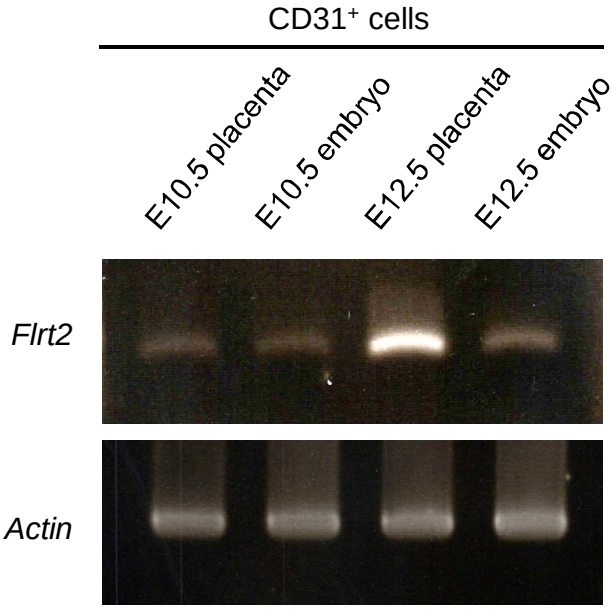

Supplementary Figure 5. Flrt2 expression in FACS-sorted CD31$^+$ endothelial cells.

Flrt2 expression in CD31$^+$ endothelial cells, determined by RT-PCR, is abundant in the placenta at embryonic day (E)12.5, compared with placentas and embryos at E10.5.

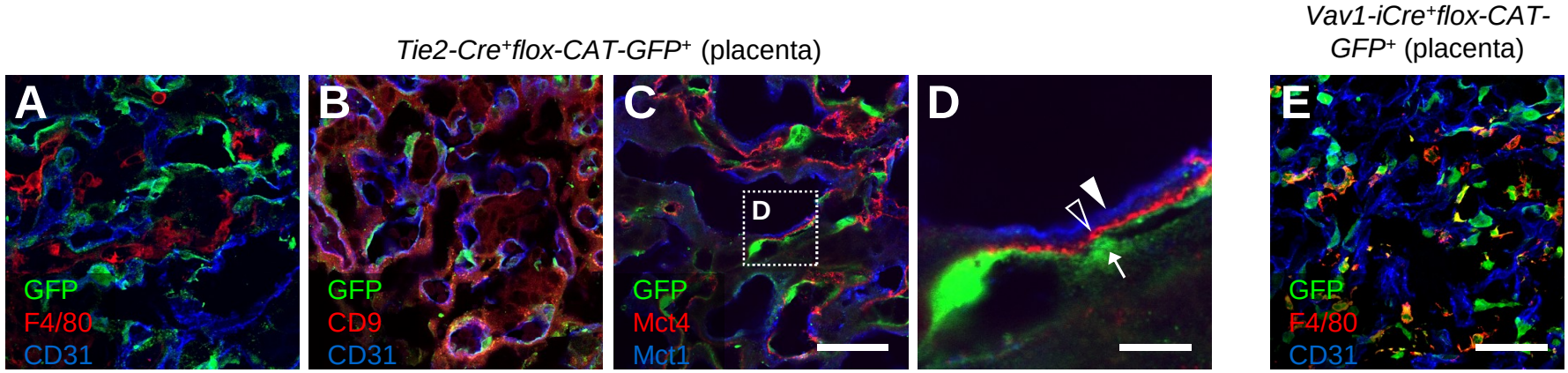

Supplementary Figure 6. Placental expression of Tie2-Cre/Vav1-iCre.

Immunohistochemistry of placental sections taken at embryonic day (E)12.5. Cre recombinase expression (indicated by the presence of green fluorescent protein) in placental endothelial cells was detected in *Tie2–Cre* (**A–D**) but not in *Vav1–iCre* (**E**) crosses. In *Tie2 – Cre* mice, GFP expression was not observed in any trophoblastic-lineage cells marked by CD9, Mct1 (closed arrowhead), or Mct4 (open arrowhead), but was restricted to endothelial cells (arrow) (**D**). Scale bars: 50 µm (**A–C, E**); 10 µm (**D**).

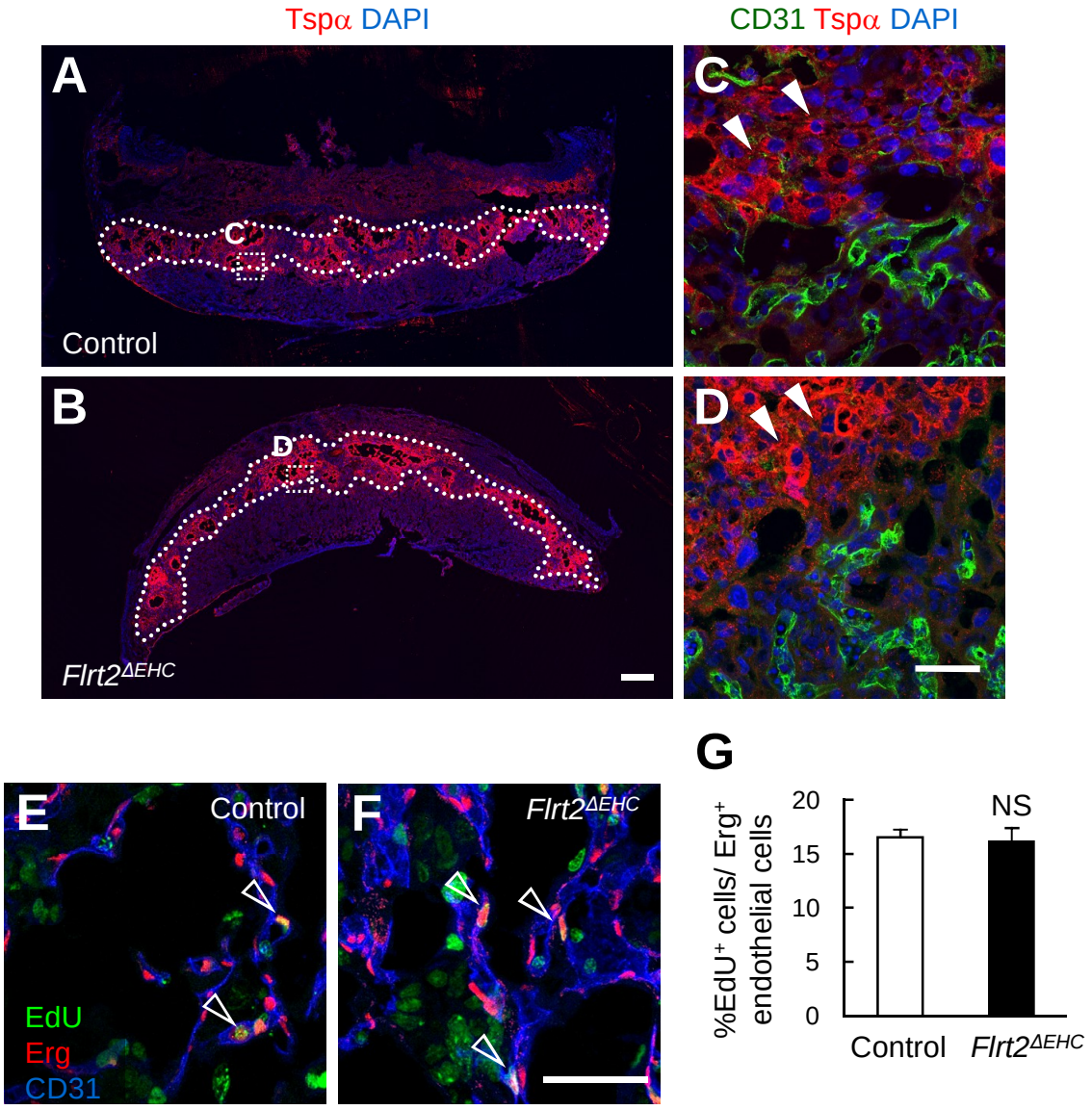

Supplementary Figure 7. Spongiotrophoblasts and endothelial proliferation are not impaired in FLRT2-deficient placentas.

(**A–G**) Immunohistochemistry and quantification of placental sections taken at embryonic day (E)12.5 (*n* = 5). Areas marked by the dotted line in **A, B** indicate the spongiotrophoblast layer. The morphology of spongiotrophoblasts (closed arrowheads in **C, D**) neighboring the labyrinth was not altered in endothelial/hematopoietic-specific *Flrt2*-knockout (*Flrt2*$^{\Delta EHC}$) mice. Open arrowheads in **E, F** indicate proliferating endothelial cells. Scale bars: 500 µm (**A, B**); 50 µm (**C–F**). NS, not significant. Data are presented as the mean ± SD.

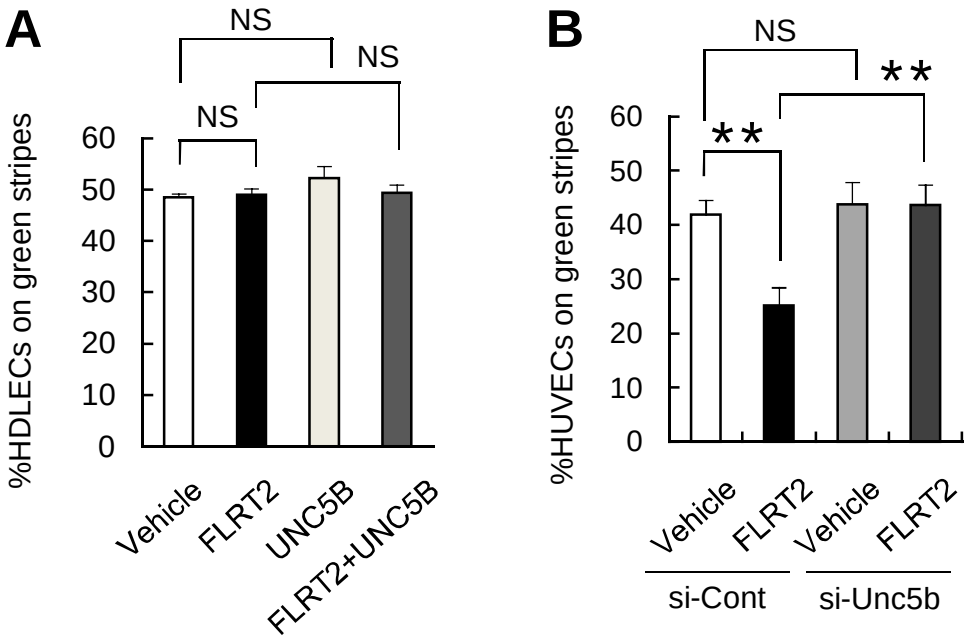

Supplementary Figure 8. FLRT2 repulses endothelial cells through the UNC5B receptor

(**A, B**) Stripe assays with human dermal lymphatic endothelial cells (HDLECs) or human umbilical vein endothelial cells (HUVECs) under small interfering RNA (siRNA)-mediated knockdown of *Unc5b*, and quantification of the results (n = 5). $^{**}P$ <0.01; NS, not significant. Data are presented as the mean ± SD.

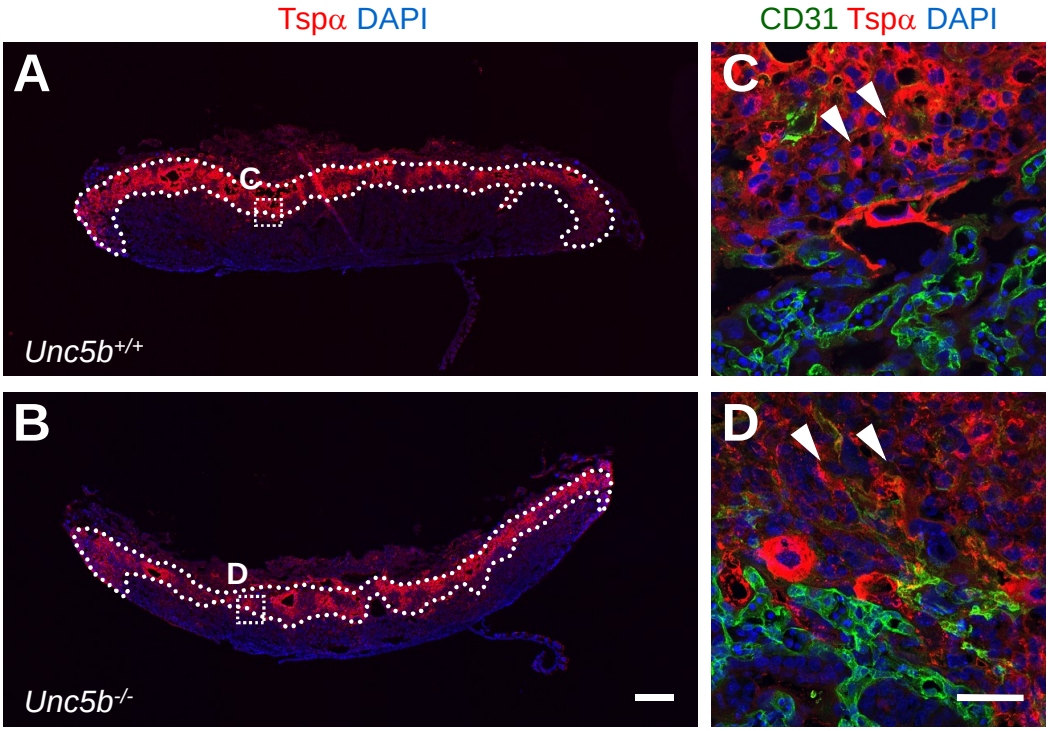

Supplementary Figure 9. Spongiotrophoblasts are not impaired in Unc5b-deficient placentas.

(**A–D**) Immunohistochemistry of placental sections taken at embryonic day (E)12.5. Areas marked by the dotted line in **A, B** indicate the spongiotrophoblast layer. The morphology of spongiotrophoblasts (closed arrowheads in **C, D**) neighboring the labyrinth was not altered in *Unc5b*$^{-/-}$ mice. Scale bars: 500 µm (**A, B**); 50 µm (**C, D**).

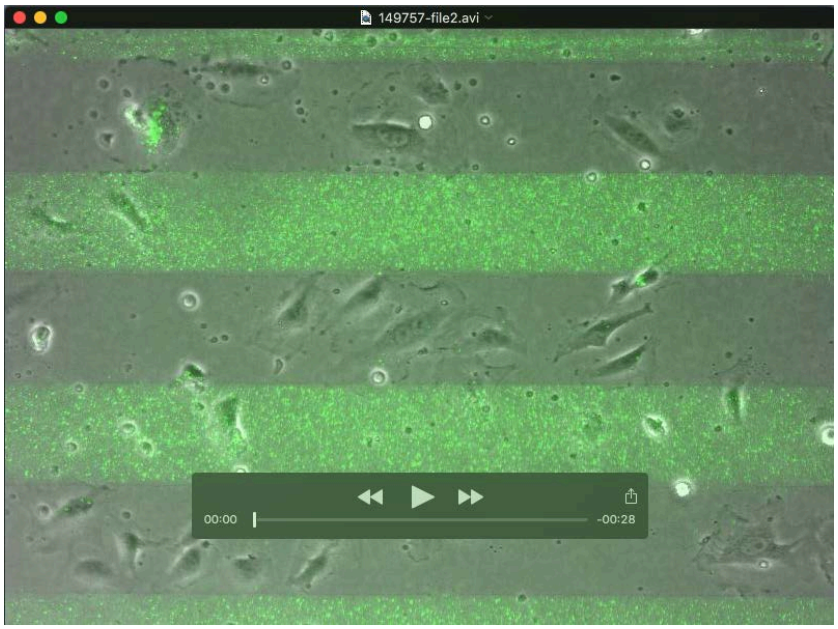

Supplementary Movie 1. FLRT2 repulses endothelial cells in vitro.

Representative movies of the stripe assay with human umbilical vein endothelial cells (HUVECs) cultured on green stripes coated with FLRT2 proteins.